*Geophys. J. Int.* (1995) **121,** 63–81

# Inversion of 3-D structural geometry using geological least-squares criteria

M. Léger,[1] J.-M. Morvan[2] and H. Rakotoarisoa[1,*]

[1]*Institut Français du Pétrole, Direction de Recherche Géophysique-Instrumentation,* BP 311, 92506 *Rueil-Malmaison, France*
[2]*Université Claude du Bernard Lyon* 1. *Institut de Mathématique et d'Informatique, Bâtiment* 101, 43 *boulevard du* 11 *Novembre,* 69622 *Villeurbanne, France*

Accepted 1994 August 17. Received 1994 August 17; in original form 1994 January 17

## SUMMARY

Oil exploration requires quantitative determination of structural geometry in sedimentary basins. This leads to back-and-forth use of geological methods, e.g. cross-section balancing and geophysical techniques, such as tomography, and the synthesis becomes tedious, especially in three dimensions. This suggests that they should be as much as possible quantitatively integrated into a single consistent framework. For this integration, we propose using inversion techniques, i.e. multicriteria optimization. We locally model a geological structure as a (*geometric*) *foliation,* the leaves of which represent deposition isochrons. We consider a geological structure as a set of foliations joined along faults and unconformities. We propose five kinds of geological data to constrain structural geometry quantitatively: dip measurements that may be available along wells, *developability* and smoothness of deposition isochrons, the directions of fold axes, and layer parallelism. Using concepts of differential geometry, we formulate these data in terms of least-squares criteria. To solve the canonical non-uniqueness problem raised by the inversion of parametric representations of geometrical objects such as foliations (many parametrizations describe the same object), we introduce the *additional criterion* method which consists of adding an *unphysical* objective function to the physical objective function, so as to make the solution unique. Assuming well trajectories and borehole correlations to be known, we optimize, with respect to these criteria, several simple structures comprising one foliation, including a field example.

**Key words:** differential geometry, inversion, sedimentary basin, structural geology, tomography, 3-D.

## 1 INTRODUCTION

In oil exploration, the quantitative determination of geological structures involves structural geology, e.g. cross-section balancing, as well as geophysics, e.g. tomography. The rise of 3-D seismic imaging induces the extension of these methods in three dimensions, but their back-and-forth use becomes very tedious. For this reason, we think that as much as possible they should be quantitatively integrated into a single consistent framework, as geophysical data are sometimes integrated (Lines, Schultz & Treitel 1988, for instance).

Cross-section balancing techniques (Suppe 1983; Moretti & Larrère 1989) are now widely used and are known to improve substantially the quality of seismic interpretations. More recently, 3-D 'structure balancing' techniques have appeared (Gratier & Guillier 1993).

Besides, tomographic inversion is an increasingly popular technique for determining geological structure (Bishop *et al.* 1985; Farra & Madariaga 1988; Haas & Viallix 1989, for instance). Geological structures are most often described by using explicit representations of layer boundaries ($z(x, y)$) and velocity fields ($v(x, y, z)$), but other methods related to CAD techniques have recently appeared and they have proven to be more powerful for the description of complex structure. For instance, Pereyra (1988) and Virieux & Farra (1991) illustrate this tendency by using spline parametric

* Now at: Stilog-IST, 163/167 avenue Georges Clémenceau, 92000 Nanterre, France.

surfaces $(x(u, v), y(u, v), z(u, v))$ or triangulations (Mallet, Jacquemin & Cheimanoff 1989). Moreover, introducing *a priori* information is known to improve the results of inversion algorithms (Jackson 1979; Tarantola 1987; Carrion, Jacovitti & Neri 1993), but the origin of this information is not very clear in practice.

Our thesis is that the so-called *a priori* information should be designed to have geological significance (Léger, Morvan & Rakotoarisoa 1991a) We propose five least-squares criteria based on geological considerations: dip measurements, *developability* and smoothness of deposition isochrons, directions of fold axes and layer parallelism. A fine description of geological structures is necessary; we use foliations via their parametric representations to do this. Using parametric representations raises a canonical non-uniqueness problem; we solve it in the inversion procedure.

Choosing the inversion approach as a theme, we first describe the geometrical modelling technique we use to describe geological structures (the unknowns). We present a geological argument that leads to geological quantities expressed in geometrical terms (the data), and the relationship between them (the forward problem). Next, physical objective functions can be derived and minimized (the inverse problem). Lastly, we describe numerical results and discuss the respective effects of these criteria on several examples and one field example.

## 2 MODELLING GEOLOGICAL STRUCTURES

Now we define how we model 'geological structures'. First, we adopt a geometrical viewpoint related to the sedimentological nature of the formations involved in oil exploration. Secondly, we adopt a functional viewpoint related to the parametric representations that we will use. Thirdly, we describe how we discretize the geometry of a structure.

### 2.1 Geometrical subsurface modelling

Our modelling of geological structures is based on the fact that all formations of oil interest comprise sedimentary rocks which may have been eroded, folded or fractured after deposition.

Since sedimentary basins have a laminated structure on graded scales, we describe them using the geometrical concept of foliation. Note that it should not be mistaken for the geological idea of foliation; indeed, this concept seems irrelevant for oil exploration situations. For this reason, we use always the geometrical word foliation in this paper. The mathematical definition of a foliation is given in Appendix A. In practice, a foliation $\mathscr{F}$ is a set of connected and disjointed surfaces, called the leaves of the foliation, which cover a volume $M$, yielding the foliated domain $(M, \mathscr{F})$. These surfaces represent sedimentation isochrons. Since this definition becomes unsuitable when faults and unconformities occur, because isochrons are not disjointed at such locations, a geological structure should be defined geometrically as a set of jointed foliations (Fig. 1).

In the following however, only one foliation is involved.

Physical properties like velocity or density could be assigned at each point for geophysical purposes. Since dip is defined everywhere in a foliation, it would be possible to introduce the *a priori* knowledge that physical properties vary slowly along dip and rapidly across dip. Furthermore, the principal axes of anisotropic physical properties could be constrained to be tangent or normal to dip.

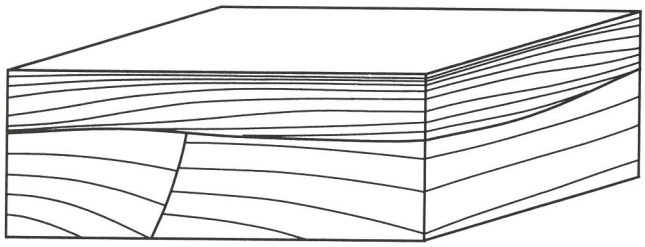

**Figure 1.** Modelling geological structures. Locally, we model sedimentary rocks by the geometrical concept of foliation: at each point, there is one and only one surface, which represents a deposition isochron. Overall, we model a geological structure as a finite set of jointed foliations separated by faults and unconformities. Moreover, physical properties could be assigned to each point for geophysical purposes.

### 2.2 Continuous functional subsurface modelling

The concept of foliation is useful for describing a geological structure locally, but it is not directly suitable for numerical uses.

Therefore, we represent foliations locally parametrically. The idea consists of parametrizing the leaves of the foliation and the points of each leaf (Fig. 2), and so defining a map $\Phi$:

$$\Phi:\{(u^1, u^2), u^3\} \in U \subset (\mathscr{R}^2 \times \mathscr{R}) \rightarrow (x^1, x^2, x^3) \in M \subset \mathscr{R}^3, \tag{1}$$

which is the parametric representation of the foliation considered. The numbers $u^1$ and $u^2$, associated with the leaf index $u^3$, are the curvilinear coordinates in parameter space $U$ of a point of foliation $(M, \mathscr{F})$ whose Cartesian coordinates are $(x^1, x^2, x^3)$ in physical space $\mathscr{R}^3$. The map $\Phi$ is assumed to be a $\mathscr{C}^2$-diffeomorphism, which means that it is one to one and that $\Phi$ and $\Phi^{-1}$ are twice continuously differentiable.

Let us emphasize that the same foliation $(M, \mathscr{F})$ can be described by an infinity of maps, even if the parameter space $U$ is specified. Clearly, there are many diffeomorphisms which conserve as a whole the foliation of $U$ by the squares $(u^3 = cst)$ and are not the identity, for instance

$$\Psi:(u^1, u^2, u^3) \in [0, 1]^3 \rightarrow \begin{pmatrix} v^1 = [u^1 + (u^1)^2]/2 \\ v^2 = [u^2 + (u^2)^2]/2 \\ v^3 = [u^3 + (u^3)^2]/2 \end{pmatrix} \in [0, 1]^3. \tag{2}$$

By construction, such maps $\Psi$ yield other parametric representations of the same foliation if composed with one particular map $\Phi$ (Fig. 3).

Parametric representations have two main advantages and two main drawbacks as compared with explicit representations in which $x^1$ and $u^1$ as well as $x^2$ and $u^2$ are identified. The first drawback is that we have to manage three functions $x^1 = \Phi^1(u^1, u^2, u^3)$, $x^2 = \Phi^2(u^1, u^2, u^3)$ and $x^3 =$

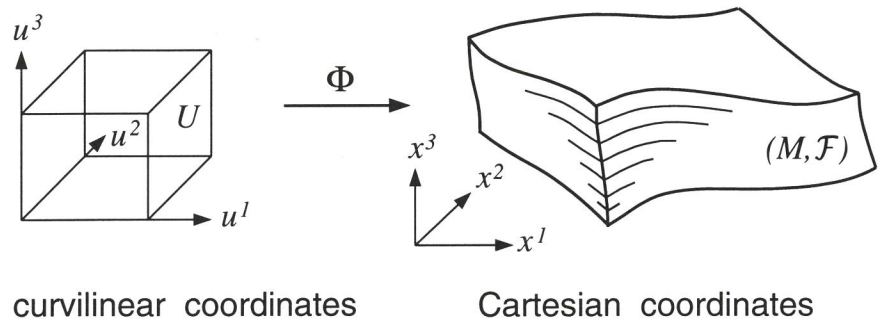


**Figure 2.** Parametric representation of a foliation. The curvilinear coordinate $u^3$ parametrizes the leaves of $\mathcal{F}$, $u^1$ and $u^2$ parametrize the points of a leaf. $x^1$, $x^2$ and $x^3$ are the Cartesian coordinates in physical space.

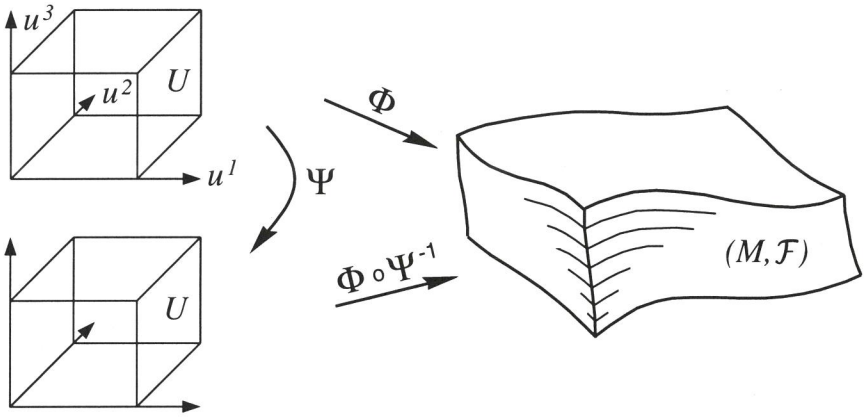


**Figure 3.** There are maps $\Psi$ which map $U$ as a whole on to itself and which conserve as a whole the foliation of $U$ by the squares $u^3 = cst$, and are not identity maps. Consequently, for any parametric representation $\Phi$ of a foliated domain $(M, \mathcal{F})$, there are other ones, $\Phi \circ \Psi^{-1}$, that describe exactly the same foliated domain (same domain $M$ and same foliation $\mathcal{F}$).

$\Phi^3(u^1, u^2, u^3)$, instead of one that would be $x^3 = f(x^1, x^2, u^3)$. The second drawback is that there are many possible parametric representations of a given foliation. Thus we have to develop special techniques in order to avoid ill-posed problems at the inversion step. The first advantage is the possibility of describing naturally recumbent folds or salt dome overhangs. The crucial advantage is that the domain of definition of functions $\Phi^1$, $\Phi^2$ and $\Phi^3$ can remain constant even if the foliation boundaries move in space. Indeed, using parametric representations is obligatory if we want to keep constant the number of discrete unknowns during the inversion process, since the geometry of the joints between foliations, i.e. faults and unconformities, is never completely and exactly known in practice.

### 2.3 Discrete functional subsurface modelling

Algorithm implementation requires the choice of a finite space of unknowns. This can be done by using a basis function decomposition of parametric representation $\Phi$

$$\Phi(u^1, u^2, u^3) = \sum_n \mathbf{p}_n B_n(u^1, u^2, u^3). \tag{3}$$

The functions $B_n(u^1, u^2, u^3)$ are the basis functions and the $\mathbf{p}_n$ are the unknowns that define a particular foliation. Note that each $\mathbf{p}_n$ is a 3-D vector because the image of $U$ by $\Phi$ is in $\mathcal{R}^3$.

It is convenient to use $B$-splines tensor-product. The parameter space $U$ is the product of three intervals of $\mathcal{R}$: $I^1 = [u^1_m, u^1_M]$, $I^2 = [u^2_m, u^2_M]$ and $I^3 = [u^3_m, u^3_M]$, on which piecewise polynomial basis functions $b^1_i(u^1)$, $b^2_j(u^2)$ and $b^3_k(u^3)$ are defined. Then the 3-D basis functions are simply

$$B_{ijk}(u^1, u^2, u^3) = b^1_i(u^1)\, b^2_j(u^2)\, b^3_k(u^3), \tag{4}$$

so that

$$(x^1, x^2, x^3) = \Phi(u^1, u^2, u^3) = \sum_{ijk} p_{ijk} b^1_i(u^1) b^2_j(u^2) b^3_k(u^3). \tag{5}$$

That is, using scalar parameters,

$$\begin{cases} x^1 = \Phi^1(u^1, u^2, u^3) = \sum_{ijk} p^1_{ijk} B_{ijk}(u^1, u^2, u^3), \\ x^2 = \Phi^2(u^1, u^2, u^3) = \sum_{ijk} p^2_{ijk} B_{ijk}(u^1, u^2, u^3), \\ x^3 = \Phi^3(u^1, u^2, u^3) = \sum_{ijk} p^3_{ijk} B_{ijk}(u^1, u^2, u^3). \end{cases} \tag{6}$$

Since we choose 1-D cubic basis functions $b^1_i(u^1)$, $b^2_j(u^2)$ and $b^3_k(u^3)$, $\Phi$ will be $\mathcal{C}^2$.

## 3 THE GEOLOGICAL DATA

We look at the geometry of sedimentary bodies from several successive viewpoints. First, sedimentology concerns sediments at the time of deposition. Secondly, tectonics or

mechanics gives an insight about their subsequent deformation. This results in a geometrical viewpoint related to structures in their present state.

We do not mean that the following assumptions are always true. For instance, **(T1)** neglects compaction and **(T2)** is clearly not appropriate for salt or shale diapirs. Moreover, we consider them at the structural scale. Hence we ignore smaller scale details which are important in seismic stratigraphy.

### 3.1 The sedimentological viewpoint

From a sedimentological viewpoint, we assume that:

**(S1)** deposition isochrons are almost parallel;
**(S2)** deposition isochrons are almost plane at deposition time.

From hypothesis **(S1)**, we derive that the deviation from parallelism at any point in a foliation, which we measure by the *convergence vector* $\mathbf{\Gamma}$ (see below), is more or less close to zero. If hypothesis **(S2)** holds true, the total curvature $K$ and mean curvature $H$ (see below), are close to zero everywhere on the leaves of a foliation.

### 3.2 The tectonic viewpoint

After deposition, sediments may be eroded, faulted or folded, but we will restrict ourselves to folding in the following. Because of their densely laminated structure, sediments can often be folded like a paper-bound book, so that the length of any curve drawn on a sheet is conserved, as well as the thickness of the sheets. In addition, the volume is conserved if the sheets remain in contact. This behaviour corresponds to the interbedding slip phenomenon. As a result, the following tectonic hypotheses about folding are sometimes acceptable (see Lisle (1992) for **(T2)**):

**(T1)** the volume of rocks is conserved;
**(T2)** the length of any curve lying on an isochron is conserved;
**(T3)** folding is not intense in the context of oil exploration;
**(T4)** the (horizontal projection of the) axis direction of folds is known; besides,
**(T5)** dip measurements are often available in wells.

### 3.3 The geometrical viewpoint

Geometers tell us that, under the above physical assumptions, the following consequences can be derived.

**(G1)** If **(S1)**, **(T1)** and **(T2)** are verified, then parallelism is conserved. This result is usually considered as obvious, referring to the paper-bound book analogy. We demonstrate it in Appendix B with the weaker assumption of area conservation instead of length conservation. We also demonstrate that not only parallelism but also deviation from parallelism is conserved under assumptions **(S1)**, **(T1)** and **(T2)**.

**(G2)** If **(S2)** and **(T2)** are verified, then $K \approx 0$ at each point of the structure in its present state. The leaves of such a foliation are called developable surfaces. Developable surfaces are cylindrical, conical or generated by the tangent to some curve in space. By *developability* we mean the property of some surfaces to be developable.

**(G3)** If **(S2)** and **(T3)** are verified, then the curvature matrix $\mathbf{C}$ (see below) is close to zero and therefore $H \approx 0$ since $K \approx 0$. The leaves of a foliation such that $H = 0$ everywhere are minimum area surfaces. Strictly speaking, no geological argument can lead to the conclusion that likely deposition isochrons should be minimum area surfaces. However, intensely folded cylindrical surfaces (Fig. 4) involve high values of mean curvature, and for this reason, we translate 'folding is not intense' as '$H \approx 0$'.

**(G4)** The intersection of a vertical plane that contains the axis direction and any leaf in the foliation yields a curve that is almost a straight line **(T4)**. In other words, the *axial curvature* $\Sigma$ of such a curve is close to zero at each point. A precise definition of the axial curvature is proposed in the next section. We do not choose the directions of fold axes as the data because this direction is undefined at each umbilic of a leaf of a foliation (an umbilic is a point around which a surface 'looks like' a sphere locally) and because this would induce severe problems at the optimization step.

**(G5)** Dip may be represented by the unit vector normal to the local foliation leaf.

Of course, the above hypotheses are only approximations to reality: first, because layers are never exactly flat and parallel after deposition, secondly, because compaction and internal strain during deformation always occur to some extent. These assumptions are convenient and powerful so

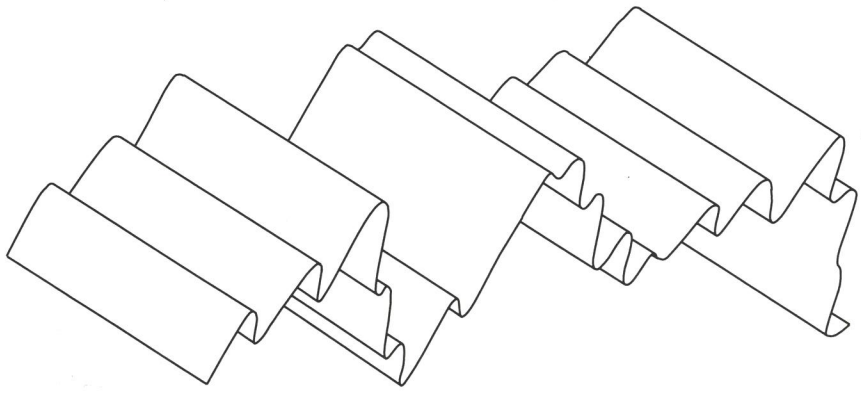

**Figure 4.** Cylindrical surfaces, and more generally developable surfaces, have zero total curvature everywhere. However, such surfaces may be intensely folded and their mean curvature $H$ is large almost everywhere. For this reason, we translate 'smooth folding' by '$H \approx 0$'.

we will use them as much as possible, just as people involved in cross-section balancing do (Moretti, Triboulet & Endignoux 1990). We will consider dip measurements, *developability*, folding intensity, *axial curvature* and layer parallelism as uncertain data: $\mathbf{N} = \mathbf{N}_0 \pm \Delta\mathbf{N}$, $K = 0 \pm \Delta K$, $H = 0 \pm \Delta H$, $\Sigma = 0 \pm \Delta\Sigma$ and $\Gamma = \mathbf{0} \pm \Delta\boldsymbol{\Gamma}$. Note that zero values are not necessary: for instance we could have $\boldsymbol{\Gamma} = \boldsymbol{\Gamma}_0 \pm \Delta\boldsymbol{\Gamma}$ where the *convergence vector* $\boldsymbol{\Gamma}_0$ points in the direction of the regional layer thinning, if any.

The geological data $\mathbf{N}$, $K$, $H$, $\Sigma$ and $\boldsymbol{\Gamma}$ will play exactly the same roles in the subsequent inversion process as picked traveltimes do in tomography.

## 4 THE FORWARD PROBLEM

The forward problem consists of evaluating synthetic data from the unknowns whereas the inverse problem consists of constraining the unknowns to be such that synthetic and observed data are as close as possible. In this section, we present the forward problem in three steps: the intrinsic or geometrical step, the continuous functional step and the discrete step.

### 4.1 The geometrical viewpoint

Assuming foliation parametric representations to be $\mathscr{C}^2$-diffeomorphisms, it is possible to define at each point $m$ in the foliation $(M, \mathscr{F})$ the plane $\mathbf{T}_m\mathscr{F}_m$ tangent to the local leaf, i.e. leaf $\mathscr{F}_m$ to which point $m$ belongs. Physical space $\mathscr{R}^3$ is endowed with the standard orientation. Hence, using the standard scalar product in $\mathscr{R}^3$, denoted $\langle\,,\rangle$, we define a unit normal vector $\mathbf{N}_m$, which is orthogonal at $m$ to $\mathbf{T}_m\mathscr{F}_m$. This results in a $\mathscr{C}^1$-differentiable unit vector field $\mathbf{N}$. The orientation of the vector field $\mathbf{N}$ is chosen to be such that it points in the direction of more recent sediments. From the orientation of $\mathscr{R}^3$ and from the orientation of $\mathbf{N}$, the orientation of each leaf in $\mathscr{F}$ can be derived. We call $\mathbf{T}\mathscr{F}$ the field of tangent planes $\mathbf{T}_m\mathscr{F}_m$. Since physical space is Euclidean, the tangent space $\mathbf{T}_mM$ to $M$ at any point $m$ in $M$ is simply $\mathscr{R}^3$ itself (like the fact that the tangent space to a piece of plane is that plane itself). The map $n : m \rightarrow \mathbf{N}_m$ is known as the Gauss mapping of the foliation.

The vector field $\mathbf{N}$ is the basic tool that will enable us to define geological synthetic data. Total and mean curvatures are related to the behaviour of $\mathbf{N}$ in directions lying in $\mathbf{T}\mathscr{F}$. Axial curvature $\Sigma$ is also related to $\mathbf{N}$. Parallelism is related to the behaviour of $\mathbf{N}$ orthogonally to $\mathbf{T}\mathscr{F}$.

We now look at the definition of operator $D$, which yields the directional derivative $D_{\mathbf{X}}\mathbf{Y}$ of a vector field $\mathbf{Y}$ in the direction of another vector field $\mathbf{X}$. The value of the vector field $D_{\mathbf{X}}\mathbf{Y}$ at any point $m$ in $M$ is

$$(D_{\mathbf{X}}\mathbf{Y})_m = \sum_{i,j} (X^i)_m \left(\frac{\partial Y^j}{\partial x^i}\right)_m \mathbf{e}_j, \tag{7}$$

where $x^1$, $x^2$ and $x^3$ are the Cartesian coordinates related to the orthonormal basis $(\mathbf{e}_1, \mathbf{e}_2, \mathbf{e}_3)$ and some origin $O$ in $\mathscr{R}^3$, and where $X^i$ and $Y^i$ are the components of the vector fields $\mathbf{X}$ and $\mathbf{Y}$ in this basis. Similarly, the directional function derivative $(\cdot)$ is defined at any point $m$ by

$$(\mathbf{X} \cdot f)_m = \sum_i (X^i)_m \left(\frac{\partial f}{\partial x^i}\right)_m, \tag{8}$$

where $\mathbf{X}$ is a $\mathscr{C}^0$ vector field and $f$ is a $\mathscr{C}^1$ function. It is easy to show that

$$(\mathbf{X} \cdot \langle \mathbf{Y}, \mathbf{Z} \rangle) = \langle D_{\mathbf{X}}\mathbf{Y}, \mathbf{Z} \rangle + \langle D_{\mathbf{X}}\mathbf{Z}, \mathbf{Y} \rangle \tag{9}$$

for any $\mathscr{C}^0$ vector field $\mathbf{X}$ and any $\mathscr{C}^1$ vector fields $\mathbf{Y}$ and $\mathbf{Z}$. As a consequence, $\langle D_{\mathbf{X}}\mathbf{Y}, \mathbf{Y} \rangle = 0$ if $|\mathbf{Y}| = 1$.

**Dip.** Let us recall that dip is represented by the unit normal vector field $\mathbf{N}$.

**Total curvature.** Since $\|\mathbf{N}\| = 1$, we have

$$\langle D_{\mathbf{X}}\mathbf{N}, \mathbf{N} \rangle = 0 = \langle D_{\mathbf{Y}}\mathbf{N}, \mathbf{N} \rangle, \tag{10}$$

and hence we can write

$$\begin{pmatrix} D_{\mathbf{X}}\mathbf{N} \\ D_{\mathbf{Y}}\mathbf{N} \end{pmatrix} = \begin{pmatrix} \langle D_{\mathbf{X}}\mathbf{N}, \mathbf{X} \rangle \langle D_{\mathbf{X}}\mathbf{N}, \mathbf{Y} \rangle \\ \langle D_{\mathbf{Y}}\mathbf{N}, \mathbf{X} \rangle \langle D_{\mathbf{Y}}\mathbf{N}, \mathbf{Y} \rangle \end{pmatrix} \begin{pmatrix} \mathbf{X} \\ \mathbf{Y} \end{pmatrix} = \mathbf{C} \begin{pmatrix} \mathbf{X} \\ \mathbf{Y} \end{pmatrix}, \tag{11}$$

where $\mathbf{X}$ and $\mathbf{Y}$ are $\mathscr{C}^0$ orthogonal unit vector fields in $\mathbf{T}\mathscr{F}$. The total curvature is the determinant of the curvature matrix $\mathbf{C}$ (which can be shown to be symmetrical),

$$K = \det(\mathbf{C}) = \langle D_{\mathbf{X}}\mathbf{N}, \mathbf{X} \rangle \langle D_{\mathbf{Y}}\mathbf{N}, \mathbf{Y} \rangle - \langle D_{\mathbf{X}}\mathbf{N}, \mathbf{Y} \rangle^2. \tag{12}$$

The eigenvalues of curvature matrix $\mathbf{C}$ are called principal curvatures and its eigenvectors are called principal directions.

**Mean curvature.** The mean curvature $H$ is a function over $(M, \mathscr{F})$ defined as follows:

$$H = -\frac{1}{2}\operatorname{trace}(\mathbf{C}) = -\frac{1}{2}(\langle D_{\mathbf{X}}\mathbf{N}, \mathbf{X} \rangle + \langle D_{\mathbf{Y}}\mathbf{N}, \mathbf{Y} \rangle), \tag{13}$$

for any $\mathscr{C}^0$ orthogonal unit vector fields $\mathbf{X}$ and $\mathbf{Y}$ in $\mathbf{T}\mathscr{F}$.

**Axial curvature.** Let $\mathbf{A}$ be a $\mathscr{C}^1$ horizontal unit vector field that represents the known direction of fold axes in the area considered. $\mathbf{A}$ is expected to vary very slowly in space. If $(\mathbf{e}_1, \mathbf{e}_2, \mathbf{e}_3)$ is an orthonormal basis in physical space $\mathscr{R}^3$, such that $\mathbf{e}_3$ is vertical, we can define another $\mathscr{C}^1$ horizontal unit vector field $\mathbf{B}$ such that $\mathbf{B} = \mathbf{A} \times \mathbf{e}_3$. Next, the cross-product of $\mathbf{B}$ and $\mathbf{N}$ yields a $\mathscr{C}^1$ vector field $\mathbf{T} = \mathbf{B} \times \mathbf{N}$ which lies in $\mathbf{T}\mathscr{F}$. The orthogonal projection of $\mathbf{T}$ on a horizontal plane is parallel to $\mathbf{A}$ (Fig. 5). Note that the modulus of $\mathbf{T}$ ranges from 0 to 1. We have $\|\mathbf{T}_m\| = 1$ at $m$ in $(M, \mathscr{F})$ if and only if $\mathbf{B}_m \in \mathbf{T}_m\mathscr{F}_m$, and $\|\mathbf{T}_m\| = 0$ if and only if $\mathbf{A}_m \in \mathbf{T}_m\mathscr{F}_m$. Finally, we define the axial curvature $\Sigma$ in the direction $\mathbf{A}$ as

$$\Sigma = \langle D_{\mathbf{T}}\mathbf{N}, \mathbf{T} \rangle. \tag{14}$$

**Convergence vector.** We introduce the *convergence vector field* $\boldsymbol{\Gamma}$ as the directional derivative of $\mathbf{N}$ in its own direction, which yields a $\mathscr{C}^0$ vector field,

$$\boldsymbol{\Gamma} = D_{\mathbf{N}}\mathbf{N}. \tag{15}$$

The convergence vector at point $m$ in $(M, \mathscr{F})$ is the value $\boldsymbol{\Gamma}_m$ of $\boldsymbol{\Gamma}$ at that point (Fig. 6). We call the quantity $\|\boldsymbol{\Gamma}_m\|$ the *convergence*. $\boldsymbol{\Gamma}$ lies in $\mathbf{T}\mathscr{F}$ since $\|\mathbf{N}\| = 1$ and $\boldsymbol{\Gamma} = D_{\mathbf{N}}\mathbf{N}$.

We denote by a parallel foliation a foliation $\mathscr{F}$ such that the convergence vector field $\boldsymbol{\Gamma}$ is zero over $M$. This means that the field lines of vector field $\mathbf{N}$ are straight lines. For this reason, we use $\boldsymbol{\Gamma}$ to measure deviation from parallelism. This definition of a parallel foliation is compatible with the usual definition of two parallel surfaces which are such that any straight line orthogonal to one is also orthogonal to the other. Indeed, a parallel foliation is such that *any* two leaves of it are parallel and the converse also holds.

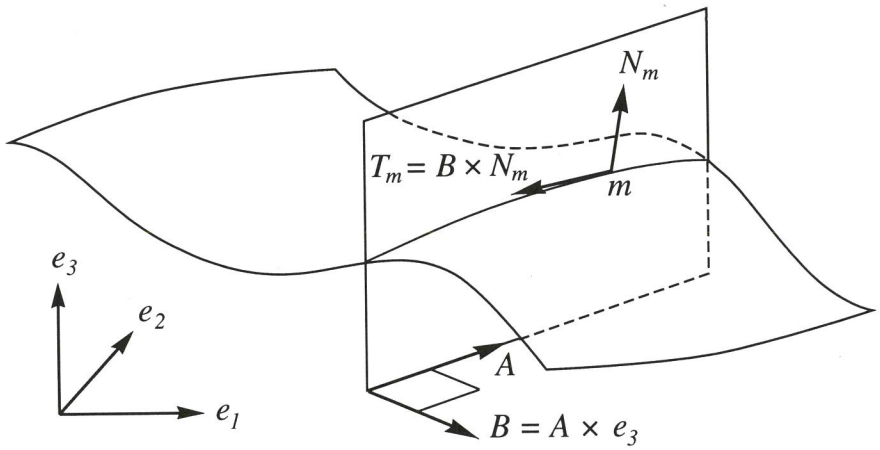


**Figure 5.** We define axial curvature $\Sigma$ as $\langle D_{\mathbf{T}}\mathbf{N}, \mathbf{T}\rangle$ where $\mathbf{N}$ is the unit vector field normal to the local leaf, $\mathbf{T} = \mathbf{B} \wedge \mathbf{N}$ and $\mathbf{B} = \mathbf{A} \wedge \mathbf{e}_3$. Unit vector field $\mathbf{A}$ is the known axis direction of folds in the horizontal plane defined by $\mathbf{e}_1$ and $\mathbf{e}_2$.

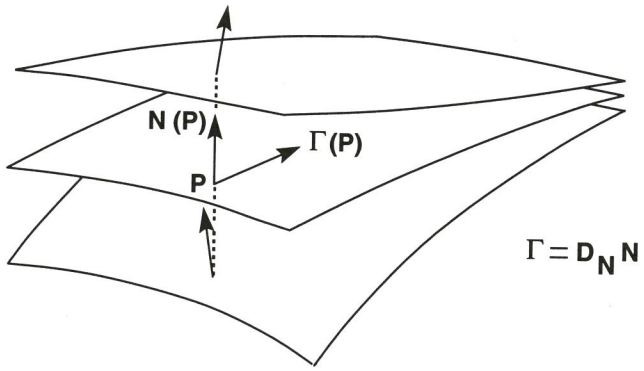


**Figure 6.** Convergence vector field $\mathbf{\Gamma}$ is the normal derivative $D_{\mathbf{N}}\mathbf{N}$ of the unit vector field $\mathbf{N}$ normal to the local leaf. It measures the deviation from parallelism at any point of a foliation since by definition $\mathbf{\Gamma} = 0$ is equivalent to local parallelism. The $L^2$ norm of $\mathbf{\Gamma}$ results in a parallelism criterion.

### 4.2 The functional viewpoint

In the previous section the quantities $\mathbf{N}$, $K$, $H$, $\Sigma$ and $\mathbf{\Gamma}$ were defined at each point of the foliation $(M, \mathcal{F})$ in physical space. Now we express them as mappings of curvilinear coordinates in $\mathbf{U}$.

**Dip.** The functional expression for dip is

$$\mathbf{N} \circ \Phi(\mathbf{u}) = \frac{\dfrac{\partial \Phi}{\partial u^1}(\mathbf{u}) \times \dfrac{\partial \Phi}{\partial u^2}(\mathbf{u})}{\left\| \dfrac{\partial \Phi}{\partial u^1}(\mathbf{u}) \times \dfrac{\partial \Phi}{\partial u^2}(\mathbf{u}) \right\|}, \tag{16}$$

where $\mathbf{N} \circ \Phi(\mathbf{u}) = \mathbf{N}(\Phi(\mathbf{u}))$ denotes unit normal $\mathbf{N}$.

**Total curvature.** It can be shown (Spivak 1979, Vol. I) that

$$K \circ \Phi = \frac{\mathcal{LN} - \mathcal{M}^2}{EG - F^2}, \tag{17}$$

where

$$\mathcal{L} = \left\langle \frac{\partial^2 \Phi}{(\partial u^1)^2}, \mathbf{N} \circ \Phi \right\rangle,$$

$$\mathcal{M} = \left\langle \frac{\partial^2 \Phi}{\partial u^1 \, \partial u^2}, \mathbf{N} \circ \Phi \right\rangle, \tag{18}$$

$$\mathcal{N} = \left\langle \frac{\partial^2 \Phi}{(\partial \mathbf{u}^2)^2}, \mathbf{N} \circ \Phi \right\rangle,$$

and where

$$E = \left\langle \frac{\partial \Phi}{\partial u^1}, \frac{\partial \Phi}{\partial u^1} \right\rangle, \quad F = \left\langle \frac{\partial \Phi}{\partial u^1}, \frac{\partial \Phi}{\partial u^2} \right\rangle, \quad G = \left\langle \frac{\partial \Phi}{\partial u^2}, \frac{\partial \Phi}{\partial u^2} \right\rangle. \tag{19}$$

**Mean curvature.** Similarly, the mean curvature $H \circ \Phi$ can be evaluated as follows:

$$H \circ \Phi = \frac{\mathcal{L}G + \mathcal{N}E - 2\mathcal{M}F}{2(EG - F^2)}. \tag{20}$$

**Axial curvature.** The expression for the axial curvature $\Sigma \circ \Phi$ is

$$(\langle D_{\mathbf{T}}\mathbf{N}, \mathbf{T}\rangle) \circ \Phi = \langle (D_{\mathbf{T}}\mathbf{N}) \circ \Phi, \mathbf{T} \circ \Phi \rangle \tag{21a}$$

$$= \langle (D_{\mathbf{B}\times\mathbf{N}}\mathbf{N}) \circ \Phi, \mathbf{B} \times \mathbf{N} \circ \Phi \rangle \tag{21b}$$

$$= \langle D_{(\mathrm{d}\Phi)^{-1}\mathbf{B}\times\mathbf{N}\circ\Phi}\mathbf{N} \circ \Phi, (\mathbf{B} \times \mathbf{N}) \circ \Phi \rangle, \tag{21c}$$

where $\mathbf{T} = \mathbf{B} \times \mathbf{N}$ and $\mathbf{B} = \mathbf{A} \times \mathbf{e}_3$. Note that $D$ represents the directional derivative in the curvilinear space in eq. (21c) whereas it represents the directional derivative in the physical space in eqs (21a) and (21b).

**Convergence vector.** From the definition of the convergence vector, we obtain

$$\mathbf{\Gamma} \circ \Phi = (D_{\mathbf{N}}\mathbf{N}) \circ \Phi, \tag{22}$$

and finally

$$\mathbf{\Gamma} \circ \Phi = D_{(\mathrm{d}\Phi)^{-1}\mathbf{N}\circ\Phi}\mathbf{N} \circ \Phi. \tag{23}$$

Note that $D$ represents the directional derivative in the curvilinear space in eq. (23) whereas $D$ represents the directional derivative in the physical space in eq. (22).

### 4.3 The discrete viewpoint

Connecting the previous expressions for synthetic data $\mathbf{N}$, $K$, $H$, $\Sigma$ and $\mathbf{\Gamma}$, which involve a parametrization $\Phi$, and the discrete expression of $\Phi$, stated in Section 2.3, yields the

discrete expression of these data. Note that this discretization refers to the parameter space, the space of the unknowns, i.e. these data depend on a finite number of spline coefficients. In the next section, another discretization will involve the data space, i.e. we will consider these data at a finite number of points.

## 5 THE GEOLOGICAL CRITERIA

We wish to find out the foliation $(M, \mathcal{F})$ such that the vector or scalar fields $\mathbf{N}$, $K$, $H$, $\Sigma$ and $\Gamma$ are as close as possible to the available data $\mathbf{N}_0$, $K_0 = 0$, $H_0 = 0$, $\Sigma_0 = 0$ and $\Gamma_0 = 0$. To do this, we choose norms $\|\cdot\|_{\mathbf{N}}$, $\|\cdot\|_K$, $\|\cdot\|_H$, $\|\cdot\|_\Sigma$ and $\|\cdot\|_\Gamma$ that will measure the distance between synthetic and available data.

### 5.1 The geometrical viewpoint

Dip, total curvature, mean curvature, axial curvature and parallelism least-squares criteria will consist in the minimization of a squared norm on the fields $\mathbf{N} - \mathbf{N}_0$, $K$, $H$, $\Sigma$ and $\Gamma$.

$$
\begin{aligned}
Q_{\mathbf{N}}(\mathcal{F}) &= \frac{1}{2}\int_{M_{\mathbf{N}}} \|\mathbf{N} - \mathbf{N}_0\|_{\mathbf{N}}^2 \, dM_{\mathbf{N}}, \\
Q_K(\mathcal{F}) &= \frac{1}{2}\int_{M} \|K\|_K^2 \, dM, \\
Q_H(\mathcal{F}) &= \frac{1}{2}\int_{M} \|H\|_H^2 \, dM, \\
Q_\Sigma(\mathcal{F}) &= \frac{1}{2}\int_{M} \|\Sigma\|_\Sigma^2 \, dM, \\
Q_\Gamma(\mathcal{F}) &= \frac{1}{2}\int_{M} \|\Gamma\|_\Gamma^2 \, dM.
\end{aligned}
\tag{24}
$$

In the first equation, $M_{\mathbf{N}}$ is the set of points in $M$ where dip measurements $\mathbf{N}_0$ are available (usually a set of wells), and the norm $\|\cdot\|$ refers to the vector space $\mathbf{T}_m M = \mathcal{R}^3$ for any $m$ in $M_{\mathbf{N}}$. These objective functions are dimensionless.

In what follows, we use $*$ instead of $\mathbf{N}$, $K$, $H$, $\Sigma$ and $\Gamma$ in order to simplify the notation.

### 5.2 The functional viewpoint

If a foliation $(M, \mathcal{F})$ is defined by a parametric representation $\Phi$, it is possible to evaluate the geological objective functions in terms of $\Phi$ by a straightforward change of variable,

$$
Q_*(\Phi) = \frac{1}{2}\int_{\mathbf{U}} \|* \circ \Phi\|_*^2 \, |\mathbf{J}_\Phi| \, d\mathbf{U}. \tag{25}
$$

In these equations, $|\mathbf{J}_\Phi|$ is the Jacobian of $\Phi$, and $* \circ \Phi$ represents quantity $*$ at point $\Phi(\mathbf{u})$ as a function of the vector of the curvilinear coordinates $\mathbf{u} = (u^1, u^2, u^3)$. The objective function related to dip is

$$
Q_{\mathbf{N}}(\Phi) = \frac{1}{2}\int_{\mathbf{U}_{\mathbf{N}}} \|(\mathbf{N} - \mathbf{N}_0)\|_{\mathbf{N}}^2 \left|\frac{d\Phi}{du^3}\right| d\mathbf{U}_{\mathbf{N}}, \tag{26}
$$

where $\mathbf{U}_{\mathbf{N}}$ is $\Phi^{-1}(M_{\mathbf{N}})$. Since $M_{\mathbf{N}}$ is a set of curves representing wells, and since $\mathbf{U}_{\mathbf{N}}$ is a set of lines $(u^1 = u^1_W, u^2 = u^2_{W_i})$ for each well $W_i$, $i \in [1, N_W]$, the Jacobian term due to the change of variable is $\left|\frac{d\Phi}{du^3}\right|$ instead of $|\mathbf{J}_\Phi|$.

### 5.3 The discrete viewpoint

Objective functions $Q_*(\Phi)$ are computed by approximating the integrals by sums,

$$
Q_*(\Phi) \approx \frac{1}{2}\sum_{u \in G_D} \|* \circ \Phi(\mathbf{u})\|_*^2 \, |\mathbf{J}_\Phi(\mathbf{u})| \, d\mathbf{U}, \tag{27}
$$

where $G_D$ is a regular grid of points $u$ in $\mathbf{U}$ and $d\mathbf{U}$ is the volume of a cell in $G_D$ in which each grid node is centred. More precisely, the curvilinear coordinates of the nodes of $G_D$ are

$$
\begin{aligned}
&u^l_i = u^l_m + \frac{2i-1}{2N^l_D}(u^l_M - u^l_m), \\
&l \in \{1, 2, 3\} \qquad 1 \le i \le N^l_D,
\end{aligned}
\tag{28}
$$

where $N^l_D$ is the number of gridpoints in direction $u^l$. Besides, we discretize set $M_{\mathbf{N}}$ using a grid $G^{\mathbf{N}}_D$ which does not need to be a subset of $G_D$. Hence, the objective function $Q_{\mathbf{N}}$ becomes

$$
Q_{\mathbf{N}}(\Phi) \approx \frac{1}{2}\sum_{G^{\mathbf{N}}_D} \|\mathbf{N} - \mathbf{N}_0\|_{\mathbf{N}}^2 \left|\frac{d\Phi}{du^3}\right| d\mathbf{U}_{\mathbf{N}}. \tag{29}
$$

As a result, the discrete data space is a vector space, each component of which is one of the three components of $\mathbf{N} \circ \Phi$ at one of the $\mathbf{N}^{\mathbf{N}}_D$ nodes of grid $G^{\mathbf{N}}_D$, or the values of $K \circ \Phi$, $H \circ \Phi$ and $\Sigma \circ \Phi$ at the nodes of $G_D$, or one of the three components of $\Gamma \circ \Phi$ at one of the $N_D = N^1_D N^2_D N^3_D$ nodes of grid $G_D$. Calling these discrete spaces $D_{\mathbf{N}}$, $D_K$, $D_H$, $D_\Sigma$ and $D_\Gamma$, we define the overall physical data space as

$$
D_\varphi = D_{\mathbf{N}} \times D_K \times D_H \times D_\Sigma \times D_\Gamma. \tag{30}
$$

The dimension of $D_\varphi$ is then $N_\varphi = 3N^{\mathbf{N}}_D + 6N_D$.

For optimization purposes, we compute the Jacobian matrices $\mathbf{J}_*(\mathbf{p})$ such that $\delta\mathbf{d}_* = \mathbf{J}_*(\mathbf{p})\delta\mathbf{p}$, where $\delta\mathbf{p}$ is a parameter perturbation around $\mathbf{p}$, and $\delta\mathbf{d}_*$ the corresponding perturbation in data space $D_*$. Hence, the overall Jacobian matrix can be written

$$
\mathbf{J}_\varphi = (\mathbf{J}_{\mathbf{N}}, \mathbf{J}_K, \mathbf{J}_H, \mathbf{J}_\Sigma, \mathbf{J}_\Gamma)^t. \tag{31}
$$

This matrix has $N_\varphi$ rows and $N_P$ columns.

### 5.4 The uncertainties

Norms $\|\cdot\|_*$ should account for the uncertainties about the $*$ quantities as evaluated by geostatistical studies in the basin considered, for instance. However, to our knowledge, such results are not yet available. Hence, we simply define these norms as weighted $L^2$ norms so that the overall physical objective function $Q_\varphi$ is

$$
Q_\varphi = \sum_* Q_* = \sum_* C_* Q_*^{L^2}, \tag{32}
$$

where $C_*$ is the weighting coefficient related to the uncertainties about $*$. These coefficients could be related to the variance $\sigma^2_*$ of $*$ and to the correlation lengths $\lambda_{*\mathbf{N}}$ and $\lambda_{*\mathbf{T}}$ in the orthogonal and tangent directions respectively,

$C_* = (\sigma_*^2 \lambda_{*\mathbf{N}} \lambda_{*\mathbf{T}}^2)^{-1}$. See Tarantola (1987) for the relationship between the choice of a norm and the corresponding covariance model.

## 6 WELL DATA

Besides uncertain distributed geological data, accurate borehole correlations are often available. In the following, well trajectories are assumed to cross each leaf of the foliation once and only once. Wells may be slanted. We describe here how we formulate this information. Moreover, in some of the subsequent numerical experiments, we need the assumption of a completely and exactly known surface in the foliation, and we also describe here its formulation since it is similar to that we use for well data.

Without loss of generality, we assign constant $u^1_{W_i}$ and $u^2_{W_i}$ values to the first and second curvilinear coordinates of all the points of every well $W_i$, and we choose the foliation's third curvilinear coordinate $u^3$ to parametrize all the curves representing wells. The information related to the well $W_i$ is then formulated as

$$\forall \mathbf{u} \in \{u^1_{W_i}\} \times \{u^2_{W_i}\} \times [u^3_m, u^3_M]; \qquad \Phi(\mathbf{u}) = \Phi_0(\mathbf{u}), \tag{33}$$

where $\Phi_0$ is some given parametric representation of the foliation.

Some of our numerical experiments need the location and shape of a leaf of $\mathcal{F}$ to be exactly known. If this leaf is defined by $u^3 = u^3_0$, we formualte this information as follows:

$$\forall \mathbf{u} \in [u^1_m, u^1_M] \times [u^2_m, u^2_M] \times \{u^3_0\}; \qquad \Phi(\mathbf{u}) = \Phi_0(\mathbf{u}), \tag{34}$$

We discretize the equality constraints of eq. (33) by applying them to $N^3_P$ points regularly located between points $(u^1_{W_i}, u^2_{W_i}, u^3_m)$ and $(u^1_{W_i}, u^2_{W_i}, u^3_M)$, where $N^3_P$ is the number of spline coefficients in the $u^3$ direction. We discretize equality constraints of eq. (34) similarly by using $N^1_P N^2_P$ points whose curvilinear coordinates $u^1$ (resp. $u^2$) are regularly located between $u^1_m$ and $u^1_M$ (resp. $u^2_m$ and $u^2_M$). Since these equality constraints should be linearly independent, we remove the closest point to the given leaf for each well, so that the total number of constraints is $N_C = N^1_P N^2_P + N_W(N^3_P - 1)$. Using eq. (6), we obtain the following system of equality constraints

$$\mathbf{Cp} = \mathbf{e}, \tag{35}$$

where $\mathbf{p}$ denotes the vector of all the parameters and $\mathbf{e}$ the vector of all the given point coordinates.

## 7 THE INVERSE PROBLEM

As stated earlier, a foliation (as well as a curve or a surface) can be described by an infinite number of parametric representations, and the physical objective function $Q_\varphi$, which we have to minimize under constraints, is primarily defined on foliations and secondarily on parametric representations. Consequently, $Q_\varphi$ will have the same value for all the parametric representations that describe the same foliation, and the inverse problem will be ill posed in terms of parametric representations even if it is well posed in terms of foliations.

To solve this problem, we propose a method, the *additional criterion method,* which is illustrated in Fig. 7, and presented in Appendix C from a mathematical viewpoint. This method is expected to meet two basic requirements (Léger, Morvan & Rakotoarisoa 1991b).

(1) To make the inversion problem as well posed in terms of parametric representations as it is in terms of foliations.

(2) To keep the physical problem unchanged.

Therefore, we design it in two steps.

(1) Definition of an *additional* objective function $Q_\alpha$ that

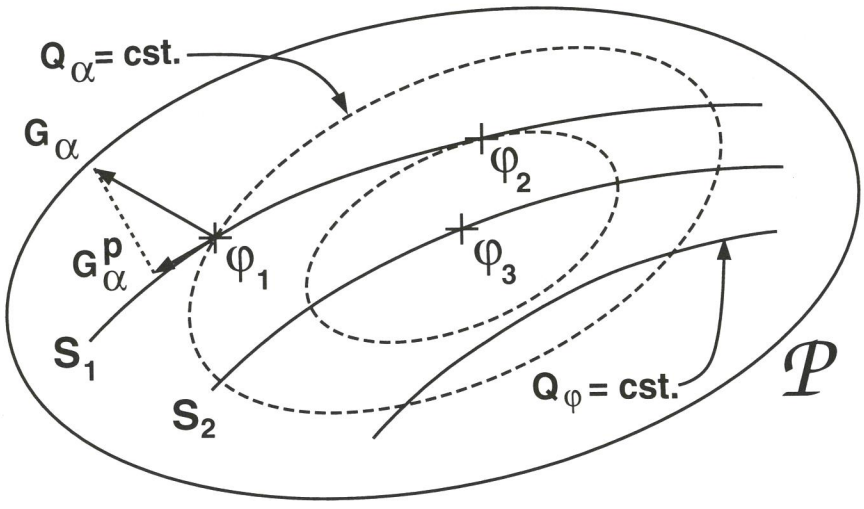


**Figure 7.** The additional criterion method for surfaces. We consider the space $\mathcal{P}$ of all parametrizations of all surfaces. Since many parametrizations represent the same surface (for instance, $\varphi_1$ and $\varphi_2$ both describe $S_1$), we may assume for simplicity that these subsets of $\mathcal{P}$ of parametrizations representing the same surface are the leaves of a foliation. Any physical objective function $Q_\varphi$ will be constant on each leaf of that foliation since data are defined on a surface. Therefore, the inverse problem is ill posed in terms of parametrizations, even if a single surface minimizes $Q_\varphi$. To make it well posed, we introduce an additional objective function $Q_\alpha$ (contours in dashed lines), but parametrization $\varphi_3$, which minimizes $Q_\alpha + Q_\varphi$, will generally not represent surface $S_1$, which minimizes $Q_\varphi$. For this reason, we project gradient $\mathbf{G}_\alpha$ of function $Q_\alpha$ on the tangent space to the local leaf, we use projected gradient $\mathbf{G}^{\mathbf{p}}_\alpha$ in the optimization process and we find parametrization $\varphi_2$. This method would work similarly for curves and we use it for foliations in this paper.

meets the first requirement by addition to the physical criterion $Q_\varphi$.

(2) Its modification so as to obtain an *unphysical* objective function $Q_\alpha^{\mathbf{p}}$ that meets both requirements by addition to $Q_\varphi$.

Since it is related to the Gauss–Newton optimization procedure, we will first recall briefly how this procedure works.

### 7.1 The Gauss–Newton procedure

The standard Gauss–Newton method consists of solving the linearized and discretized problem iteratively,

$$\mathbf{J}_\varphi^t \mathbf{J}_\varphi \delta\mathbf{p} = -\mathbf{J}_\varphi^t \delta\mathbf{d}_\varphi, \tag{36}$$

under the equality contains $\mathbf{Cp} = \mathbf{e}$, where $\delta\mathbf{p}$ is the model modification vector, $\delta\mathbf{d}_\varphi$ is the physical data misfit, $\mathbf{J}_\varphi$ the Jacobian matrix of $\mathbf{d}_\varphi(\mathbf{p})$ around the current model, with $^t$ denoting transpose.

This problem cannot be solved since there are degrees of freedom in the parameter space that cannot be determined by physical data, despite the equality constraints, because of the multiplicity of the parametric representations for one foliation. For this reason, we now introduce an additional criterion so as to obtain a well-posed problem in terms of parametric representations.

### 7.2 The additional objective function $\mathbf{Q}_\alpha$

At the first step of the method, we define additional data

$$\alpha^{ijk} = \frac{\partial^2 \Phi^i}{\partial u^j \, \partial u^k}(\mathbf{u}), \tag{37}$$

where $\Phi^i(\mathbf{u})$ is the $i$th Cartesian coordinate of the point whose curvilinear coordinates are $\mathbf{u} = (u^1, u^2, u^3)$. For each vector $\mathbf{u}$, quantities $\alpha^{ijk}(\mathbf{u})$ build an 18-component vector $\boldsymbol{\alpha}(\mathbf{u})$ that represents the 'synthetic data' in the inversion context (18 using symmetries, 27 otherwise). Next we define the 'observed data' as $\boldsymbol{\alpha}_0(\mathbf{u}) = 0$ for any $\mathbf{u}$ in $U$. Choosing a $L^2$ norm on the vector field $\boldsymbol{\alpha} - \boldsymbol{\alpha}_0 = \boldsymbol{\alpha}$ yields the additional objective function

$$Q_\alpha(\Phi) = \frac{1}{2}\int_U \|\boldsymbol{\alpha}\|_\alpha^2 \, dU, \tag{38}$$

where $\|\cdot\|_\alpha = C_\alpha \|\cdot\|_{L^2}$. The numerical value of $C_\alpha$ is chosen to avoid problems related to the limited precision of computers. The practical effect of minimizing $Q_\alpha(\Phi)$ is to smooth out the mesh associated with $\Phi$ on the foliation $(M, \mathcal{F})$ it represents.

### 7.3 Physical and unphysical parameters

At the second step of the method, we need to modify $Q_\alpha(\Phi)$ to keep it from having any physical significance, since the foliation described by the parametrization that minimizes $Q_\varphi(\Phi)$ could be different from the foliation described by the parametrization that minimizes $Q_\varphi(\Phi) + Q_\alpha(\Phi)$. To do this, we distinguish which parameters are unphysical and which parameters are physical.

Unphysical parameters correspond to perturbations of a parametric representation such that points are moved tangentially to the local leaf. Conversely, physical parameters correspond to perturbations such that points are moved transversally to the local leaf (Fig. 8a). However, some combinations of physical parameters may be unphysical. This happens if all the points of a leaf in a foliation are moved to another single leaf (Fig. 8b). The situation is somewhat different at the boundaries of a foliation since the local leaf may no longer be the only physically significant surface. At these locations, unphysical parameters correspond to perturbations that lie at the intersection of the tangent planes to all physically significant surfaces, which may be the local leaf (deposition isochron) or a piece of the foliation's boundary (fault or unconformity in practice). In Fig. 9, the black (white) arrows span the vector space of the unphysical (physical) perturbations at several kinds of points.

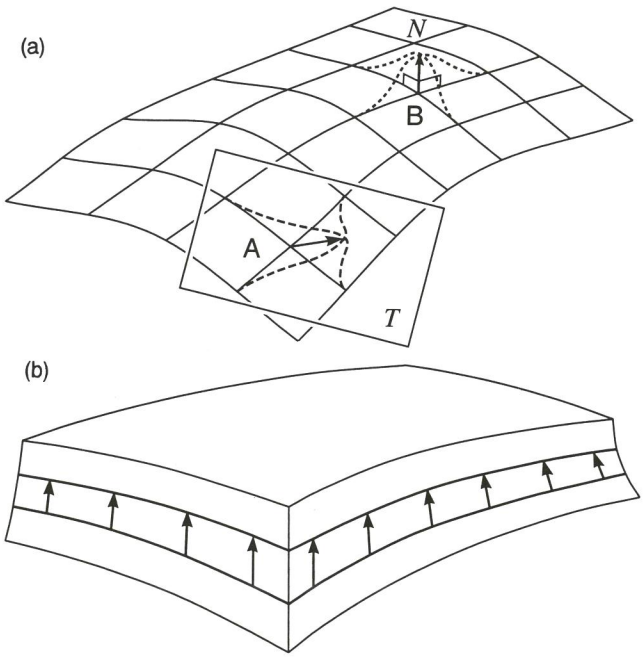


**Figure 8.** Physical and unphysical perturbations. (a) If a point is moved but remains on the same leaf of a foliation, this foliation is unchanged despite its modified parametric representation (dashed lines). Purely physical perturbations of a point are orthogonal to the local leaf (dotted lines). (b) Some combinations of physical perturbations may be unphysical since they conserve the foliation. They correspond to a change of variable on the curvilinear coordinate that parametrizes the foliation leaves.

### 7.4 The modified Gauss–Newton procedure

This distinction between physical and unphysical perturbations can be transposed to the parameter space via the following change of variables.

First, we choose a grid of points $G_P$ in $U$ such that the set of the Cartesian coordinates of grid $\Phi(G_P)$ in $(M, \mathcal{F})$ is equivalent to vector $\mathbf{p}$ of the discrete parameters, i.e. spline coefficients.

$$G_P = \left\{ (u^1, u^2, u^3); u^i \in \{u_1^i, \ldots, u_{N_{pi}}^i\}, \right.$$
$$\left. u_j^i = u_m^i + (u_M^i - u_m^i)\frac{j-1}{N_{pi}-1} \right\}. \tag{39}$$

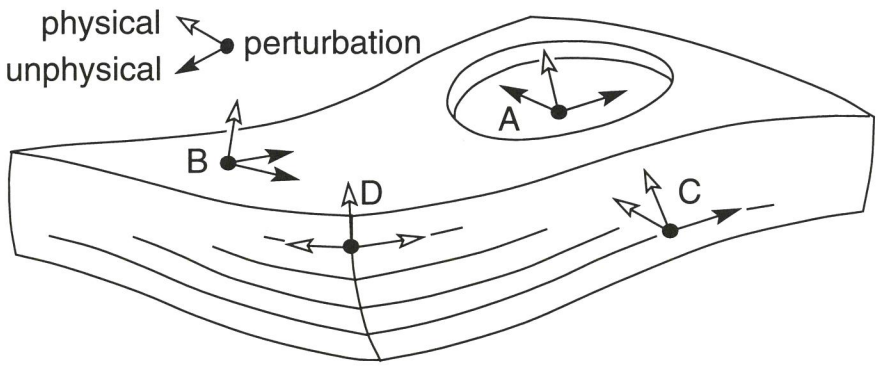


**Figure 9.** Unphysical perturbations (black arrows) are tangent to *all* physically significant surfaces. At points *A* and *B*, the only physically significant surface is the local leaf. At *C*, another one is the face, which may represent a fault. At *D*, all perturbations are physical (white arrows).

Secondly, we attribute a specific base $(\boldsymbol{\varepsilon}_1, \boldsymbol{\varepsilon}_2, \boldsymbol{\varepsilon}_3)$ to each of the nodes of grid $\Phi(G_P)$ such that

$$\boldsymbol{\varepsilon}_i = \left(\frac{\partial\Phi^1}{\partial u^i}, \frac{\partial\Phi^2}{\partial u^i}, \frac{\partial\Phi^3}{\partial u^i}\right), \; i \in \{1, 2\}, \; \boldsymbol{\varepsilon}_3 = \boldsymbol{\varepsilon}_1 \times \boldsymbol{\varepsilon}_2. \tag{40}$$

The set of the coordinates of grid $\Phi(G_P)$ nodes related to the frames $(O, \boldsymbol{\varepsilon}_1, \boldsymbol{\varepsilon}_2, \boldsymbol{\varepsilon}_3)$ builds a vector $\mathbf{q}$ such that $\mathbf{q} = \mathbf{L}\mathbf{p}$. This results in a new Jacobian matrix

$$\mathbf{J}_{\alpha\mathbf{q}} = \mathbf{J}_\alpha \, \mathbf{L}^{-1}. \tag{41}$$

Keeping the additional criterion from having any physical significance now simply consists of zeroing the columns of $\mathbf{J}_{\alpha\mathbf{q}}$ that are related to physical parameters, using a projection matrix $\mathbf{P}$:

$$\mathbf{J}^{\mathrm{p}}_{\alpha\mathbf{q}} = \mathbf{J}_\alpha \cdot \mathbf{L}^{-1} \cdot \mathbf{P}. \tag{42}$$

Coming back to the spline coefficient space, the projected Jacobian matrix becomes

$$\mathbf{J}^{\mathrm{p}}_\alpha = \mathbf{J}_\alpha \cdot \mathbf{L}^{-1} \cdot \mathbf{P} \cdot \mathbf{L}, \tag{43}$$

and the modified linearized problem then becomes

$$[\mathbf{J}^{\mathrm{t}}_\varphi \mathbf{J}_\varphi + (\mathbf{J}^{\mathrm{p}}_\alpha)^{\mathrm{t}} \mathbf{J}^{\mathrm{p}}_\alpha]\delta\mathbf{p} = \mathbf{J}^{\mathrm{t}}_\varphi \delta\mathbf{d}_\varphi + (\mathbf{J}^{\mathrm{p}}_\alpha)^{\mathrm{t}} \delta\mathbf{d}_\alpha. \tag{44}$$

Appendix C demonstrates that the modified gradient $\mathbf{G}^{\mathrm{p}}_\alpha = \mathbf{J}^{\mathrm{p}}_\alpha(\mathbf{p}) \cdot \delta\mathbf{d}_\alpha$ of the objective function $Q_\alpha$ is the gradient of some objective function $Q^{\mathrm{p}}_\alpha$ that we call an *unphysical objective function.* We also demonstrate that the optimization of a foliation for $Q_\varphi$ is equivalent to the optimization of a parametric representation for $Q_\varphi + Q^{\mathrm{p}}_\alpha$. In addition, Appendix D shows two numerical inversion results that illustrate the necessity of the projection step in the additional criterion method.

Note that we never computed the objective function $Q_\varphi + Q^{\mathrm{p}}_\alpha$ which we minimized.

This method has been designed and can be implemented completely independently of the physical criteria and in harmony with the Gauss–Newton procedure.

### 7.5 Optimization with constraints

The linearized problem with constraints is solved by using the Lagrange multipliers technique. The linear system which is actually solved is the following:

$$\begin{pmatrix} \mathbf{J}^{\mathrm{t}}\mathbf{J} & \mathbf{C}^{\mathrm{t}} \\ \mathbf{C} & \mathbf{0} \end{pmatrix} \begin{pmatrix} \delta\mathbf{p} \\ \boldsymbol{\lambda} \end{pmatrix} = \begin{pmatrix} \mathbf{J}^{\mathrm{t}}\delta\mathbf{d} \\ \mathbf{e} \end{pmatrix}, \tag{45}$$

where $\mathbf{J} = \begin{pmatrix} \mathbf{J}_\varphi \\ \mathbf{J}^{\mathrm{p}}_\alpha \end{pmatrix}$, $\delta\mathbf{d} = \begin{pmatrix} \delta\mathbf{d}_\varphi \\ \delta\mathbf{d}_\alpha \end{pmatrix}$ and where $\boldsymbol{\lambda}$ is the vector of the Lagrange multipliers. Besides, a linear search is carried out with a user-supplied reduction factor $\beta$. That is, if $\delta\mathbf{p}^{(k)}$ is the model modification resulting from the linearized problem at the $k$th iteration, we define the next current model as: $\mathbf{p}^{(k+1)} = \mathbf{p}^{(k)} + \beta\delta\mathbf{p}^{(k)}$.

### 7.6 Uncertainty analysis

After convergence has been reached, an uncertainty analysis may be carried out. For a least-squares problem without constraints such that the map $\mathbf{p} \to \mathbf{d} = f(\mathbf{p})$ is linear, the solution $\tilde{\mathbf{p}}$ equals the mathematical expectation $\bar{\mathbf{p}}$ of the *a posteriori* Gaussian probability density function in the parameter space, and the covariance matrix is $\mathbf{C}_{\mathbf{p}} = (\mathbf{J}^{\mathrm{t}}\mathbf{J})^{-1}$ according to the above notation. If map $f$ is not linear, the Gaussian property in the parameter space becomes an approximation, and the second derivatives of map $f$ should appear in the expression for $\mathbf{C}_{\mathbf{p}}$ (see Tarantola (1987) p. 194 for details). We consider the linearized problem in the following.

If a foliation is moved in space, all objective functions remain the same, including the additional one. Consequently, matrix $\mathbf{J}^{\mathrm{t}}\mathbf{J}$ is not invertible, and equality constraints $\mathbf{C}\mathbf{p} = \mathbf{e}$ (well data) need to be taken into account. Let us consider a perturbation $\delta\mathbf{p} = \mathbf{p} - \bar{\mathbf{p}}$ in parameter space such that $\mathbf{C}\delta\mathbf{p} = 0$; then $\mathbf{C}\mathbf{p} = \mathbf{e}$ since $\mathbf{C}\bar{\mathbf{p}} = \mathbf{e}$. Matrix $\mathbf{C}$ (resp. $\delta\mathbf{p}$) can be split into $\mathbf{C}_1$ and $\mathbf{C}_2$ (resp. $\delta\mathbf{p}_1$ and $\delta\mathbf{p}_2$) such that $\mathbf{C}_1\delta\mathbf{p}_1 + \mathbf{C}_2\delta\mathbf{p}_2 = 0$ and such that $\mathbf{C}_2$ is invertible. Therefore:

$$\delta\mathbf{p} = \begin{pmatrix} \delta\mathbf{p}_1 \\ \delta\mathbf{p}_2 \end{pmatrix} = \begin{pmatrix} \mathbf{Id} \\ -\mathbf{C}_2^{-1}\mathbf{C}_1 \end{pmatrix} \delta\mathbf{p}_1 = \mathbf{A}\delta\mathbf{p}_1, \tag{46}$$

where $\delta\mathbf{p}_1$ corresponds to the unconstrained parameters. Similarly, we split the Jacobian matrix $\mathbf{J}$ into $\mathbf{J}_1$ and $\mathbf{J}_2$:

$$\delta\mathbf{d} = \mathbf{J}_1\delta\mathbf{p}_1 + \mathbf{J}_2\delta\mathbf{p}_2 = (\mathbf{J}_1 - \mathbf{J}_2\mathbf{C}_2^{-1}\mathbf{C}_1)\delta\mathbf{p}_1. \tag{47}$$

Then, the Hessian matrix

$$\mathbf{H}_1 = (\mathbf{J}_1 - \mathbf{J}_2\mathbf{C}_2^{-1}\mathbf{C}_1)^t(\mathbf{J}_1 - \mathbf{J}_2\mathbf{C}_2^{-1}\mathbf{C}_1) \quad (48)$$

of the overall objective function is invertible in the unconstrained parameter subspace, which yields covariance matrix $\mathbf{C}_1 = \mathbf{H}_1^{-1}$. From eq. (46), we derive covariance matrix $\mathbf{C}_\mathbf{p}$ in the overall parameter space: $\mathbf{C}_\mathbf{p} = \mathbf{A}\mathbf{C}_1\mathbf{A}^t$. Using $\bar{\mathbf{p}}$ and $\mathbf{C}_\mathbf{p}$, any vector quantity $\mathbf{Q} = \mathbf{L}\mathbf{P}$ can be estimated ($\mathbf{P}$ is the random vector variable of the parameters and $\mathbf{L}$ is a matrix):

$$\bar{\mathbf{q}} = \mathbf{L}\bar{\mathbf{p}}; \qquad \mathbf{C}_\mathbf{q} = \mathbf{L}\mathbf{C}_\mathbf{p}\mathbf{L}^t. \quad (49)$$

For instance, vector $\mathbf{Q}$ may correspond to the Cartesian coordinates of a point in a foliation. Then matrix $\mathbf{C}_\mathbf{q}$ is $3 \times 3$ and the points $\bar{\mathbf{q}} \pm \sqrt{\lambda_i}\,\mathbf{V}_i$ represent the three error bars, where $\lambda_i$ (resp. $\mathbf{V}_i$) are the eigenvalues (resp. eigenvectors) of $\mathbf{C}_\mathbf{q}$.

By referring to Section 7.3, we may expect that two such error bars will lie in the tangent plane and will be controlled by the weight $C_\alpha$ of the additional criterion, whereas the third error bar will be orthogonal to the tangent plane and will be controlled by the weights $C_*$ of the physical criteria and the well constraints. We will check this in the next section.

## 8 NUMERICAL RESULTS

We now give several examples of inversion which use the above geological criteria. These results might seem unrealistic since they involve only one foliation, whereas geological structures are generally made of several, but this complexity is beyond the scope of this paper and is left to the future.

First, we give simple examples in which one leaf of the foliation and two wells are assumed to be known, and we discuss what the effect of the geological criteria is. Next, we give more realistic examples involving no given foliation leaf.

### 8.1 The effect of the geological criteria

We now give four examples in which two wells are available and the top surface of the foliation is given.

#### *8.1.1 Description of the problem*

The problem consists of finding one foliation $\mathcal{F}$ that is subject to the following constraints:

(1) the foliation minimizes the physical criterion $Q_\varphi$.

(2) two vertical wells are given and they cross all the leaves of $\mathcal{F}$ once and only once at known points. No dip is known except when stated otherwise;

(3) the top leaf of the foliation is known;

(4) the lateral faces of $\mathcal{F}$ (those that are not the upper or lower leaf) have no particular location or shape.

Conditions (1) and (2) have a clear physical meaning and they are relevant to oil-exploration situations. Condition (3) does not correspond to realistic situations because a geological interface is never completely and exactly known in practice. Since we do not yet have any geological or geophysical criteria that could constrain the shape of a fault or of an unconformity, the lateral faces of the foliation are arbitrarily constrained by using the additional criterion. This is the meaning of 'condition' (4). Nevertheless, all these conditions are necessary for us to have a simple, stand-alone and well-posed problem. Condition (3), especially, is necessary because, for instance, well data and parallelism are compatible with many foliations. In realistic situations, this condition is replaced by a regularity criterion which leads to a well-posed problem if at least three non-aligned boreholes are given. It may be also replaced by Kriging.

The discretization parameters are $N_P^1 = 10$, $N_P^2 = 6$, $N_P^3 = 4$ in the parameter space and $N_D^1 = 18$, $N_D^2 = 10$, $N_D^3 = 6$ in each scalar data space. This results in 720 parameters and 25 920 scalar data for all the criteria including the unphysical one. Conditions (2) and (3) result in 108 equality constraints. Computing time per iteration is about 20 min for all criteria on a Cray YMP computer. Convergence is usually achieved within three to five iterations.

#### *8.1.2 Effect of parallelism criterion*

Figure 10 shows the result of the inversion with $Q_\varphi = Q_\Gamma$ and $C_\Gamma = 1$. The borehole correlations are such that no exactly parallel foliation can meet well constraints. Foliation leaves are sharply curved in the vicinity of each well, thus showing a 'cone-effect'.

#### *8.1.3 Effect of developability criterion*

Figure 11 shows the inversion result with $Q_\varphi = Q_\Gamma + Q_K$ and $C_\Gamma = 1$ and $C_K = 200$. As expected, foliation leaves are quite developable and even cylindrical in this case. This picture shows three parts. Between wells, the surfaces are almost plane but they are slanted and converge to the right. On both sides, however, the foliation is quite parallel and horizontal. This results in a 'dihedral-effect', i.e. a fold *en chevron*, which is visible in the vicinity of each well.

#### *8.1.4 Effect of smoothness criterion*

Figure 12 shows the inversion result with $Q_\varphi = Q_\Gamma + Q_K + Q_H$ and $C_\Gamma = 1$, $C_K = 1$ and $C_H = 1$. As expected, the foliation leaves are smoothed, so that well locations are not obvious from just looking at the shape of the surfaces.

Figure 13 is similar to the previous figure but the curvature criteria are heavily weighted. As a result, foliation leaves are almost plane. A careful examination of the result shows that the structure is the superposition of a weak anticline and a weak syncline. We interpret the anticline as the effect of the parallelism criterion, which tries to make the convergence vector a constant over all the foliation. The syncline is due to the mean curvature criterion, which tries to make each surface as curved in any direction as it is in the orthogonal direction on the other side of the surface. The total curvature criterion should then make all the surfaces plane but it seems to fail to do so, despite the fact that it is highly weighted and that planes are the only surfaces such that $K = H = 0$ everywhere. We explain this fact as follows. Since $K$ is the determinant of curvature matrix $\mathbf{C}$, we can write $K = c_1 \cdot c_2$ where $c_1$ and $c_2$ are principal curvatures. Therefore, differentiating $K$ gives $dK = c_1 \cdot dc_2 + dc_1 \cdot c_2$,

and we notice that $dK = 0$ if $c_1 = c_2 = 0$, which is exactly the case for planes. Hence, no first-order perturbation of a plane will have any first-order effect on $K$, that is, $\mathbf{J}_K = 0$. Therefore, the effect of the total curvature criterion vanishes for planes since the Hessian matrix $\mathbf{H}_K = (\mathbf{J}_K)^t \mathbf{J}_K$ as well as the gradient $\mathbf{G}_K = (\mathbf{J}_K)^t \delta \mathbf{d}_K$ both become zero.

*8.1.5 Effect of axial curvature*

In this example, the top surface is not assumed to be known. Moreover, four wells are given instead of two as in the previous examples. One point is given at the centre of the top surface. This corresponds to 51 equality constraints.

As stated before, the total curvature objective function is strongly non-quadratic. As a result, local minima may be expected. Figs 14 and 15 illustrate this possibility since the well constraints and the physical criterion $Q_\varphi$ to be optimized are exactly the same in both cases. It appears that introducing the total curvature criterion consists of saying 'there are well-shaped folds', i.e. 'extensive dip measurements in the foliation make a thin line on a stereographic chart'. Figs 14 and 15 demonstrate that several directions of folds are sometimes possible. Since the direction of fold axes is usually known in practice, only one is likely. The axial curvature criterion enables the right one to be chosen. Using the model shown in Fig. 14 as the initial model, the result shown in Fig. 15 can be obtained within five iterations by optimizing $Q_\varphi = Q_\Gamma + Q_K + Q_H + Q_\Sigma$ and the proper axis direction in $Q_\Sigma$. Similarly, Fig. 14 can be obtained from Fig. 15.

This demonstrates that using the fold axis direction criterion substantially reduces the problem of local minima.

*8.1.6 Effect of dip*

Common sense suggests, and numerical results confirm, that the introduction of dip information can improve the estimate of the structure, especially if only a few wells are available. Fig. 16 shows the result of the same inversion as Fig. 12, but dip measurements have been added along the two wells. The angle between dip and the plane of the boreholes is 45 degrees.

*8.1.7 Summary*

Table 1 sums up the effect of the geological criteria. It gives the value of the unweighted objective functions $Q_*^{L^2}$ as a function of the weighting coefficients $C_*$. To be clearer, we also give the values of $R_\Gamma = \langle \|\Gamma\|^2 \rangle^{-\frac{1}{2}}$, $R_K = \langle K^2 \rangle^{-\frac{1}{4}}$, $R_H = \langle H^2 \rangle^{-\frac{1}{2}}$ and $R_\Sigma = \langle \Sigma^2 \rangle^{-\frac{1}{2}}$, $\langle \cdot \rangle$ denoting the average over the entire foliation. Fig. 17 illustrates the significance of these various radii of curvature. Table 1 also gives the value of $\theta = 2 \arctan [(\langle \|\mathbf{N} - \mathbf{N}_0\|^2 \rangle^{1/2}/2]$ in degrees. This angle measures the discrepancy between the given dip $\mathbf{N}_0$ and the corresponding dip of the optimal foliation.

**Table 1.** For each of Figs 10–14 and Fig. 16, this table gives the values of the weighting coefficients $C_*$ and the values of the unweighted objective functions $Q_*^{L^2}$ after the last iteration. The values of $Q_*^{L^2}$ can be interpreted in terms of several kinds of lengths $R_*$, which are defined in the text and illustrated in Fig. 17.

| Fig. | 10 | 11 | 12 | 13 | 14 | 16 |
|---|---|---|---|---|---|---|
| $C_N$ | — | — | — | — | — | 100 |
| $C_K$ (m) | 0 | 200 | 1 | 70 | 50 | 1 |
| $C_H$ ($m^{-1}$) | 0 | 0 | 1 | 50 | 1 | 1 |
| $C_\Sigma$ ($m^{-1}$) | 0 | 0 | 0 | 0 | 1 | 0 |
| $C_\Gamma$ ($m^{-1}$) | 1 | 1 | 1 | 1 | 1 | 1 |
| $Q_N^{L^2}$ | — | — | — | — | — | .0083 |
| $Q_K^{L^2}$ ($m^{-1}$) | .42 | .000021 | .024 | .0022 | .080 | .021 |
| $Q_H^{L^2}$ (m) | 8.7 | 3.9 | 1.4 | .010 | 24. | .41 |
| $Q_\Sigma^{L^2}$ (m) | 13. | .0034 | 2.0 | 0.65 | .29 | 1.8 |
| $Q_\Gamma^{L^2}$ (m) | 3.7 | 5.3 | 5.0 | 10. | .96 | 8.8 |
| $\theta$ | — | — | — | — | — | 2.1 |
| $R_K$ (m) | 7.0 | 84. | 14. | 27. | 15. | 15. |
| $R_H$ (m) | 11. | 16. | 28. | 330. | 52. | 52. |
| $R_\Sigma$ (m) | 9.1 | 580. | 23. | 41. | 24. | 24. |
| $R_\Gamma$ (m) | 17. | 14. | 15. | 10. | 11. | 11. |
| $N_{iter}$ | 5 | 6 | 5 | 6 | 8 | 5 |

## 8.2 More realistic examples

*8.2.1 A weakly folded structure*

Figure 18 shows the result of an inversion in which five wells and the direction of fold axes are given, and $Q_\varphi = Q_K + Q_H + Q_\Sigma + Q_\Gamma$ is optimized with $C_K = 50$, $C_H = 1$, $C_\Sigma = 1$ (given axis direction visible on top) and $C_\Gamma = 1$. No dip is known. One well is deviated. An anticlinal trap is visible on the top surface.

*8.2.2 A sharply folded structure*

It is possible to recover a salt dome flank with reverse dips, a rim syncline and a turtleback structure with only four wells (Fig. 19). Dips are available along them. The choice of an initial model with horizontal layers illustrates the fact that it *may* not be close to the solution. On the other hand, the algorithm converged after 12 iterations, due to the strong non-linearity of the problem.

*8.2.3 A field example*

Figure 20 displays part of a map compiled by Bodou *et al.* (1975) of an anticline outcropping on a rocky short. We tried to recover it by using only a portion of available data, keeping the rest for checking the result. Fig. 21 shows a perspective view of the computed structure. The cross-section (left of Fig. 20) shows good agreement between computed dips (italics) and given dips (regular), except at its ends. At point A, we explain the discrepancy by a lower scale fold which is visible at ($x = 100$, $y = 65$) and smoothed by the inversion. At point B, the origin of the discrepancy is less clear, although a fault is known to exist along this flank of the fold.

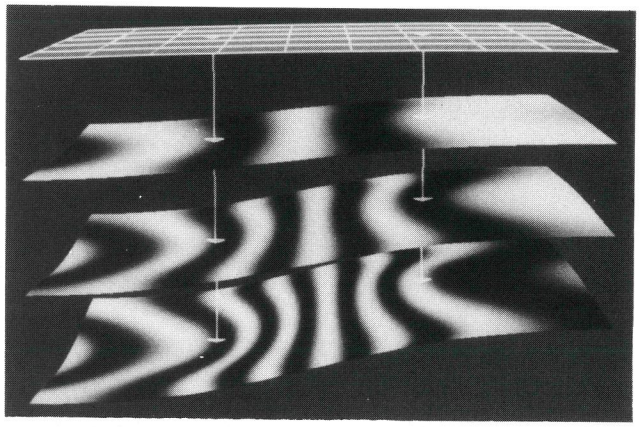

**Figure 10.** Parallelism criterion is optimized. 'Cone effects' are visible near the wells.

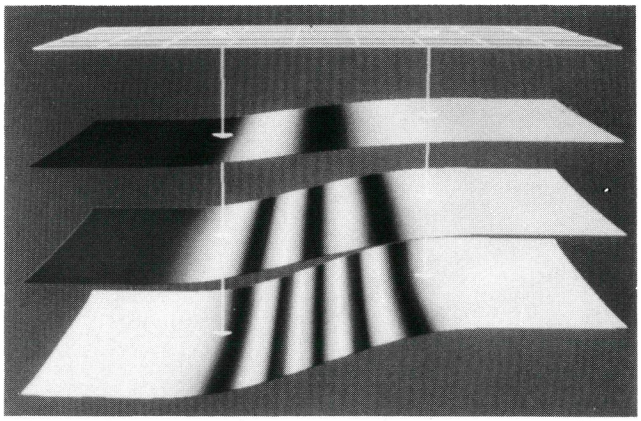

**Figure 11.** Parallelism and total curvature criteria are optimized. Foliation leaves become almost cylindrical but 'dihedral effects' are visible near the wells.

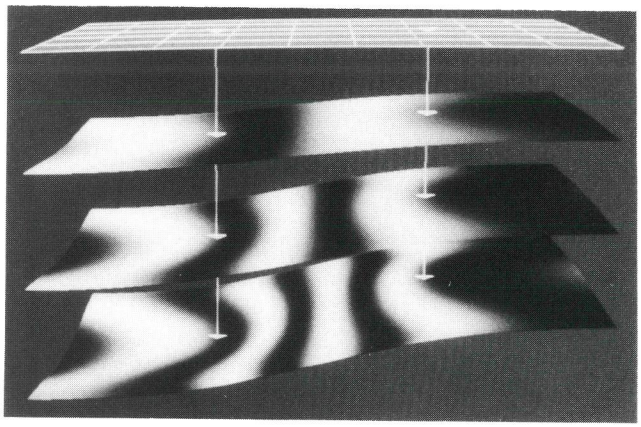

**Figure 12.** Owing to the mean curvature criterion, foliation leaves become smooth.

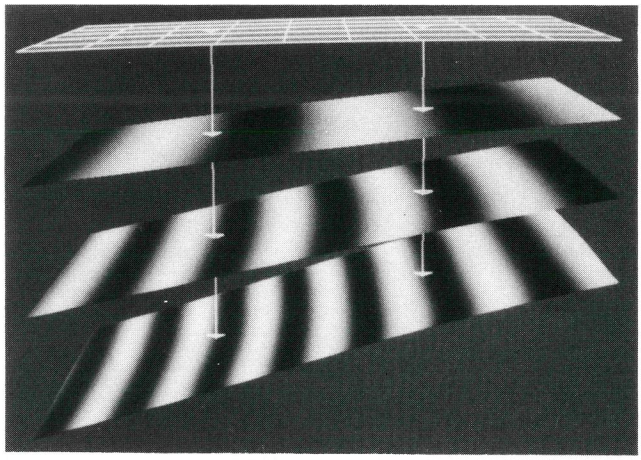

**Figure 13.** If heavily weighted, the total and mean curvature criteria make the foliation leaves almost plane.

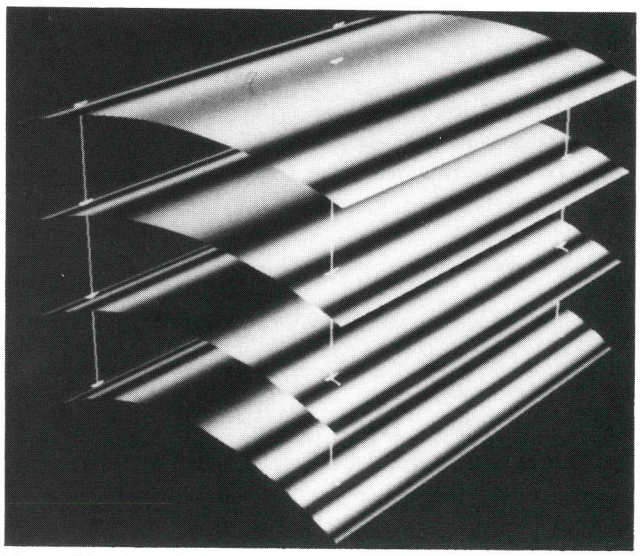

**Figure 14.** The axial curvature criterion can be used to choose the axis direction of folds if several solutions are possible (Figs 14 and 15 show distinct local minima).

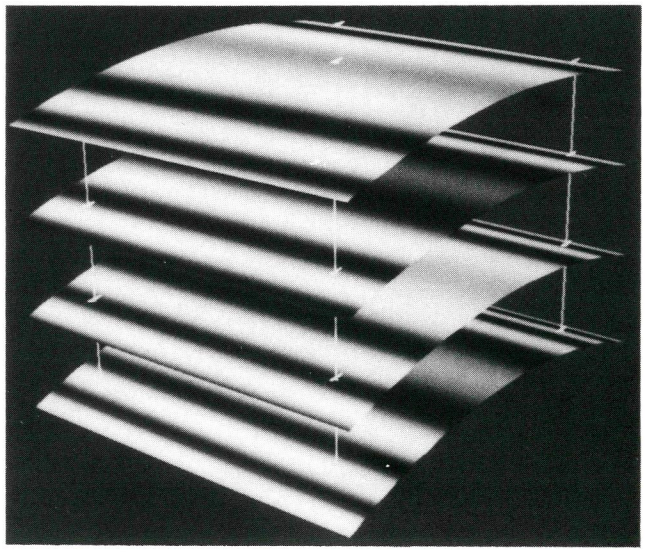

**Figure 15.** With another axis direction, this model can be obtained from Fig. 14 as the initial model.

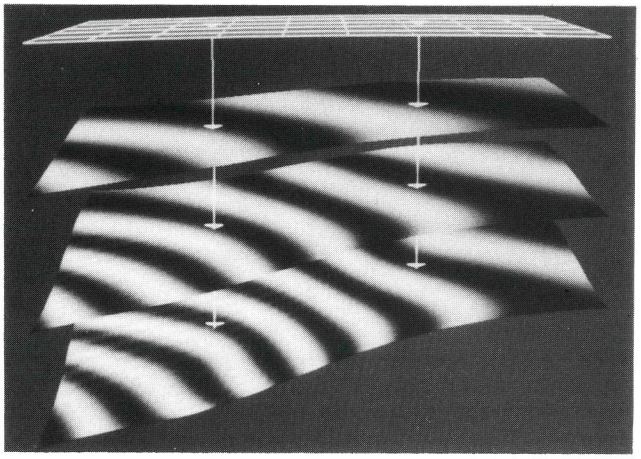

**Figure 16.** This result is similar to that in Fig. 12 but dips are introduced along wells.

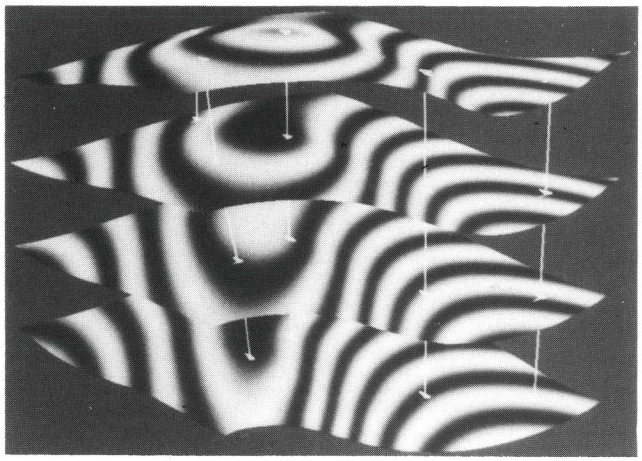

**Figure 18.** Five wells and geological criteria may yield a plausible structure. One well is deviated.

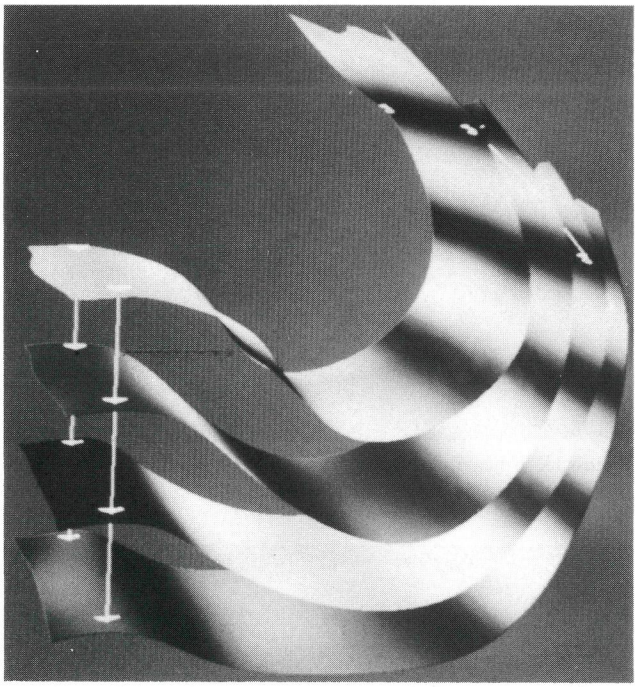

**Figure 19.** Four wells and dip logs yield this salt dome flank, rim syncline and turtleback structure within 12 iterations from a horizontal initial model.

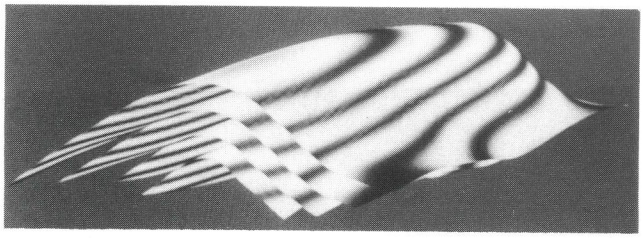

**Figure 21.** Perspective view of the computed anticline behind the ($x = 40$) vertical plane.

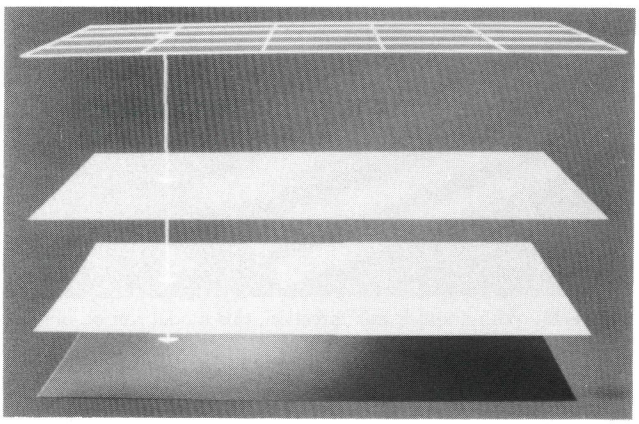

**Figure D1.** This foliation results from the optimization of a parallelism criterion, including the projection step (initial model shown in Fig. D2).

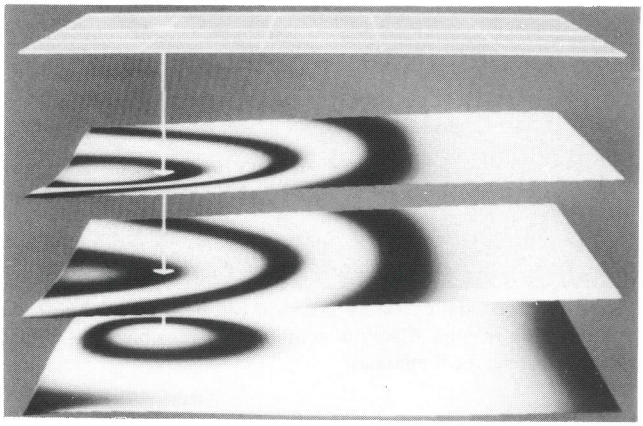

**Figure D2.** Same as Fig. D1, but the projection step has been 'forgotten'. The result is obviously not satisfactory (initial model shown in Fig. D1).

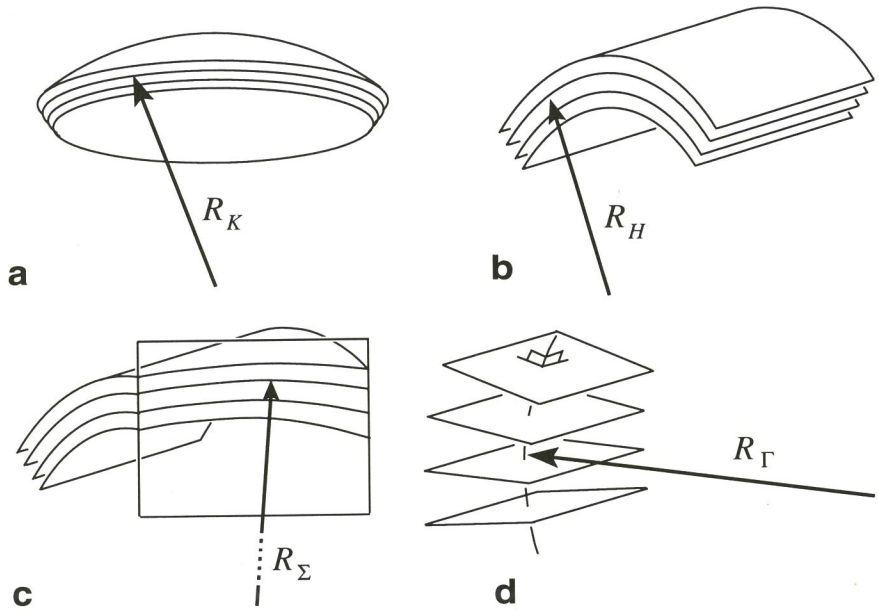


**Figure 17.** Significance of the various radii of curvature $R_K$ (a), $R_H$ (b), $R_\Sigma$ (c) and $R_\Gamma$ (d) for simply shaped foliations.

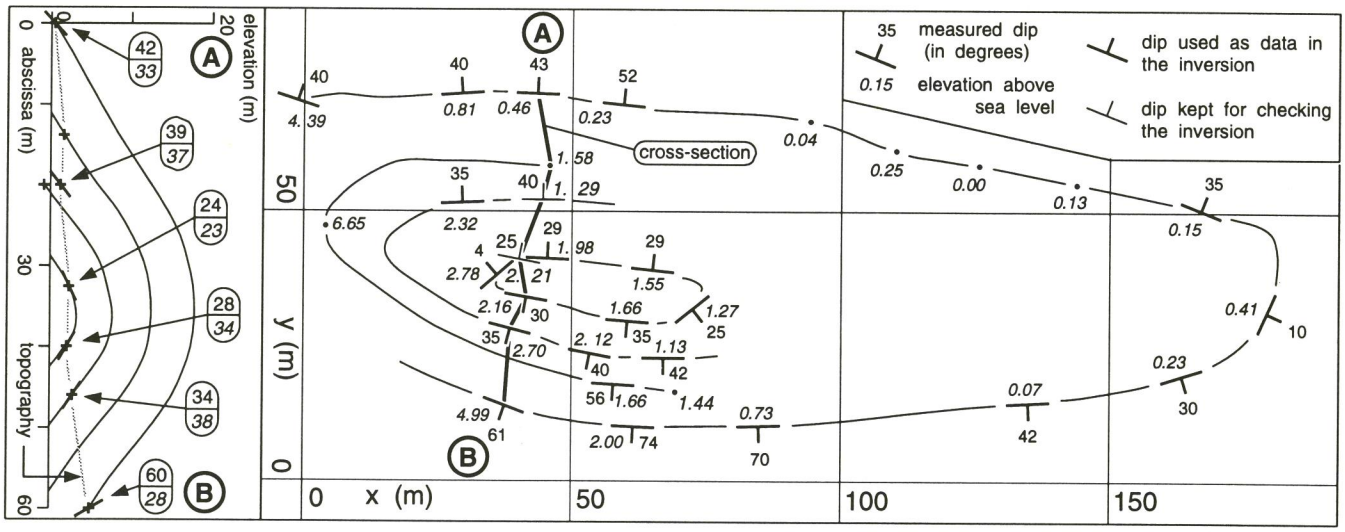


**Figure 20.** Map of a 100 m scale anticline outcropping on a rocky shore in Spain (after Bodou *et al.* 1975). We used position data via equality constraints and dip data via least-squares criteria. Cross-section A–B illustrates the match between the computed structure and data (roman = measured dips, italics = computed dips).

### 8.3 *A posteriori* study

We used the model shown in Fig. 12 (with only 360 parameters) in order to check the uncoupling between the physical criteria and the unphysical one. Using the method described in Section 7, we have computed the error bars at 32 points in the foliation.

Figure 22 shows, as a function of weight $C_\alpha$ assigned to the unphysical criterion, the histogram of the normalized values of the squared length of these error bars, i.e. variances. Normalization consists of dividing each variance by its value for $C_\alpha = 100$. Consequently, the influence of $C_\alpha$ is enhanced visually, since the variability of the variances for the position of the different points is removed. There are five classes per order of magnitude. Fig. 22 clearly demonstrates that there is a wide range of values for $C_\alpha$ such that, first, the normal variances are constant, and second, the tangent variances are proportional to $C_\alpha^{-1}$. Moreover, Fig. 23 shows the independence between the optimal value of the physical cost functions and $C_\alpha$ for a wide range of its value. These numerical results confirm the theory stated in Appendix C and assess the superiority of our additional criterion technique over standard regularizations. Indeed, minimizing $Q_\varphi + \varepsilon Q_\alpha$, with the smallest

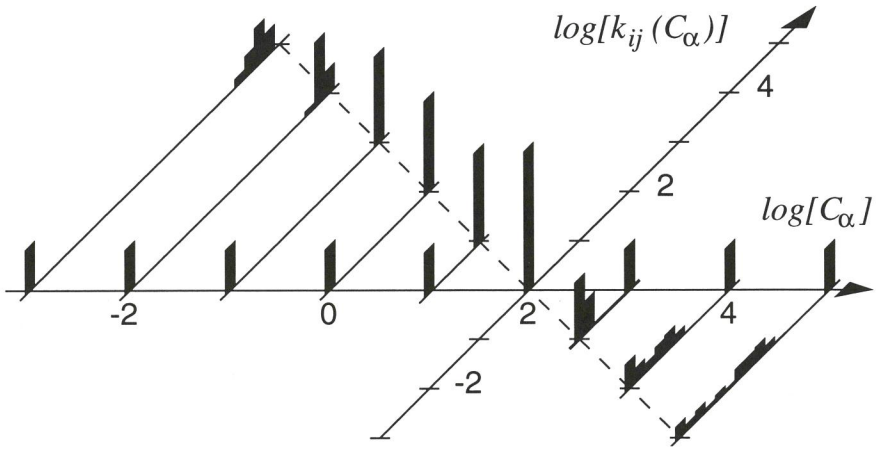


**Figure 22.** Since the three Cartesian coordinates $x$, $y$, $z$ of a point depend on curvilinear coordinates, a $3 \times 3$ covariance matrix represents the uncertainties about the position of that point. $V_{ij}(C_\alpha)$ is the $j$th eigenvalue of that matrix at the $i$th point. Since the weight $C_\alpha$ of the unphysical criterion should have no influence on the physical solution, $k_{ij}(C_\alpha) = V_{ij}(C_\alpha)/V_{ij}(100)$ should equal 1 for all physical variances which are related to orthogonal error bars. On the other hand, $k_{ij}(C_\alpha)$ should be proportional to $C_\alpha^{-1}$ for unphysical variances, which are related to tangential error bars. The histograms of normalized variances $k_{ij}(C_\alpha)$ for 32 points show that this is true for a wide range of values of $C_\alpha$. This demonstrates that the physical problem is not disturbed by the unphysical criterion.

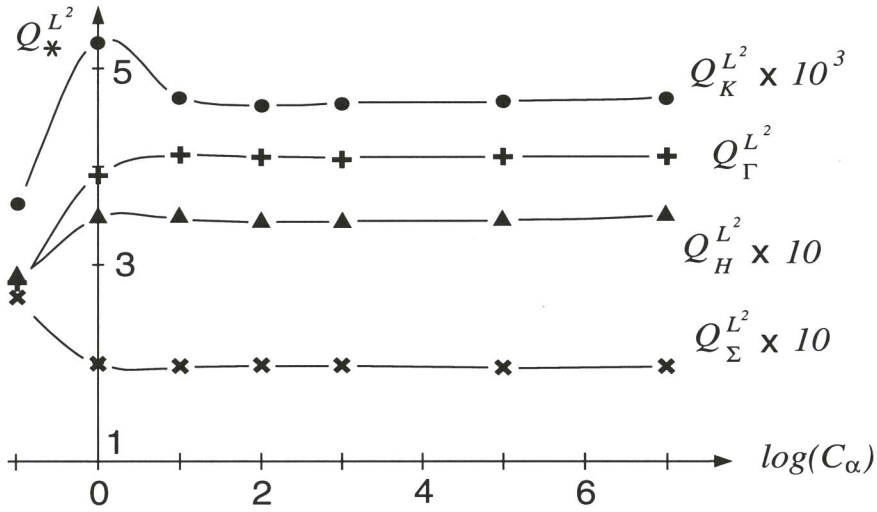


**Figure 23.** For a large range in $C_\alpha$, the physical objective functions have the same optimal values, whatever the value of the weight $C_\alpha$ may be.

possible $\varepsilon$, leads to the following dilemma: the linear system is ill conditioned if $\varepsilon$ is negligible, whereas the original physical problem is altered if it is not.

## 9 CONCLUSIONS

The geometrical concept of foliation is suitable to make a local description of geological structures in sedimentary basins. It leads to a simple and reliable definition of parallelism and deviation from parallelism. Moreover, it would be easy to correlate the shape of the velocity or density heterogeneities with the trend of local dip since dip is defined everywhere in a foliation. The description of foliations via parametric representations should make it possible to consider faults and unconformities as unknown surfaces, just as deposition isochrons are.

Simple but quantitative geological information can be translated into geometrical terms. Indeed, differential geometry turns out to yield many valuable ways of examining geometrical aspects of geological structures: we demonstrate that constant bed length and volume folding conserves layer parallelism, which is well known, and also deviation from parallelism, which seems to be a new result.

Dip measurements, which are often available in wells, yield the unit vector normal to the local leaf of the foliation. Fold developability is the nullity of the total curvature, which measures to what extent folds are 'well shaped', at any point of any leaf of the foliation. Fold smoothness is the nullity of the mean curvature. Knowing the fold axis direction for developable folds implies the nullity of the axial curvature, which measures to what extent folds are properly oriented. Finally, layer parallelism is the nullity, over all the foliation considered, of the convergence vector, which points in the direction of layer thinning.

Since this information is only an approximation to reality, a least-squares formulation is suitable for taking uncertainties into account. The optimization of the geological structure with respect to these criteria yields satisfactory results if the corresponding objective functions are properly weighted. Accurate borehole correlations, which are often available in practice, can be handled via equality constraints.

The inversion problem is always ill posed in terms of parametric representations because of their multiplicity for one foliation. To overcome this difficulty, we propose a general method that works in two steps. First a least-squares criterion smoothes out the mesh associated with parametric representation. Secondly, it is modified so that the physical inverse problem is unchanged. This method can be implemented in harmony with the standard Gauss–Newton optimization procedure.

We plan to improve this toolkit of geological least-squares criteria by adding other criteria that would constrain the shape of the faults. We will have to join several foliations so as to obtain more realistic and complex geological structures. This research is a contribution towards the partial but quantitative integration of geology and geophysics via multicriteria optimization methods.

## ACKNOWLEDGMENTS

We would like to thank J.-P. Cattin and L. Nguyen Luc for their valuable help in graphic matters. We also thank J. Brac who implemented the spline routines that we used. M. L. warmly thanks K. Marfurt for the fruitful discussions that occurred during his stay at IFP in 1988.

The research described in Léger & Rakotoarisoa (1990) was carried out as a part of the Prestack Structural Interpretation consortium project (PSI). The authors hereby acknowledge the support provided by the sponsors of this project.

## REFERENCES

Bishop, T.N., Bube, K.P., Cutler, R.T., Langan, R.T., Love, P.L., Resnick, J.R., Shuey, R.T., Spindler, D.A. & Wyld, H.W., 1985. Tomographic determination of velocity and depth in laterally varying media, *Geophysics,* **50,** 903–923.

Bodou, P., Henry, J., Jean, F., Masse, P., Meynot, C., Trémolières, P. & Zinszner, B., 1975. Étude des Déformations Structurales: les Plis de Liandres (Province de Santander, Espagne). SNPA Report (in French).

Carrion, P., Jacovitti, G. & Neri, A., 1993. Gaussian and non-Gaussian tomographic modelling via simulated annealing, *J. Seism. Explor.,* **2,** 189–204.

Farra, V. & Madariaga, R., 1988. Non-linear reflection tomography, *Geophys. J.,* **95,** 135–147.

Gratier, J.-P. & Guillier, B., 1993. Compatibility constraints on folded and faulted strata and calculation of total displacement using computational restoration (UNFOLD program), *J. Struct. Geol.,* **15,** 391–402.

Haas, A. & Viallix, J.R., 1989. Stochastic inversion by ray continuation: application to seismic tomography, *Geophys. Prospect.,* **37,** 337–356.

Jackson, D.D., 1979. The use of *a priori* data to resolve non-uniqueness in linear inversion, *Geophys. J.,* **57,** 137–157.

Léger, M. & Rakotoarisoa, H., 1990. Optimum design of the geologic structure: study of a 3-D parallelism criterion, in *60th Annual SEG Meeting, Expanded Abstracts,* pp. 351–354.

Léger, M., Morvan, J.-M. & Rakotoarisoa, H., 1991a. Inversion of 3D geologic structures using parallelism, developability and smoothness least-squares criteria, in *61st Annual SEG Meeting, Expanded Abstracts,* pp. 959–962.

Léger, M., Morvan, J.-M. & Rakotoarisoa, H., 1991b. Inversion of parametric representations of geometrical objects: a general method for solving the canonical nonuniqueness problem, in *61st Annual SEG Meeting, Expanded Abstracts,* pp. 955–958.

Lines, L.R., Schultz, A.K. & Treitel, S., 1988. Cooperative inversion of geophysical data, *Geophysics,* **53,** 8–20.

Lisle, R.J., 1992. Constant bed-length folding: three dimensional geometrical implications, *J. Struct. Geol.,* **14,** 245–252.

Mallet, J.L., Jacquemin, P. & Cheimanoff, N., 1989. GOCAD Project: Geometric modeling of complex geologic surfaces, in *59th Annual SEG Meeting, Expanded Abstracts,* pp. 126–128.

Moretti, I. & Larrère, M., 1989. Computer-aided construction of balanced geological cross-sections, *Geobyte,* 16–24.

Moretti, I., Triboulet, S. & Endignoux, L., 1990. Some remarks on the geometrical modeling of geologic deformations, in *Petroleum and Tectonics in Mobile Belts,* ed. Letouzey, J., Technip, Paris.

Pereyra, V., 1988. Two-point ray tracing in complex 3D media, in *58th Annual SEG Meeting, Expanded Abstracts,* pp. 1056–1060.

Spivak, M., 1979. *A Comprehensive Introduction to Differential Geometry,* 2nd edn, 5 Vols, Publish or Perish, Inc., Houston, TX.

Suppe, J., 1983. Geometry and kinematics of fault bend folding, *Am. J. Sci.,* **283,** 684–721.

Tarantola, A., 1987. *Inverse Problem Theory,* Elsevier, Amsterdam.

Virieux, J. & Farra, V., 1991. Ray tracing in 3D isotropic complex media: an analysis of the problem, *Geophysics,* **56,** 2057–2069.

## APPENDIX A: DEFINITION OF A (GEOMETRICAL) FOLIATION

Since geometers define foliations as a set of connected and disjointed submanifolds covering a manifold, we first review the definition of finite dimensional manifolds and submanifolds (see Spivak (1979), Vol. I, for further details).

An $n$-dimensional *manifold* $M$ is a set on which a family of charts $\{O_i, \Psi_i, U_i\}_{i \in I}$ is defined. The $O_i$ are subsets of $M$ and cover it (Fig. A1). The $U_i$ are open subsets of the normed vector space $\mathcal{R}^n$, and the $\Psi_i$ are homeomorphisms (bicontinuous one-to-one mappings). Moreover, for any $i$ and $j$, map $\Psi_i \circ \Psi_j^{-1}$ is a homeomorphism.

In addition, if all the $\Psi_i \circ \Psi_j^{-1}$ maps are $\mathcal{C}^k$-diffeomorphisms (a one-to-one mapping which is $\mathcal{C}^k$-differentiable as well as its inverse), with $k \geq 1$, then $M$ is an $n$-dimensional, *$\mathcal{C}^k$-differentiable manifold,* or, for short, a $(\mathcal{C}^k, n)$-manifold. Moreover, an $n$-dimensional tangent vector space $\mathbf{T}_m M$ can be defined at each point $m$ in $M$.

A *$(\mathcal{C}^k, p)$-submanifold* $S$ of a $(\mathcal{C}^k, n)$-manifold $M$ is a subset of $M$ such that, at any point $m$ of $S$, there exists a chart $(O_i, \Psi_i, U_i)$ of $M$ such that $m \in O_i$ and $\Psi_i(S \cap O_i) = U_i \cap F$, where $F$ is a $p$-dimensional vector subspace of $\mathcal{R}^n$ (Fig. A2). The integer $p$ is the dimension of $S$ and $n - p$ is the codimension of $S$ in $M$. In $\mathcal{R}^3$ considered as a manifold, a $(\mathcal{C}^k, 1)$-submanifold is a curve and a $(\mathcal{C}^k, 2)$-submanifold is a surface.

A foliated manifold $(M, \mathcal{F})$ is a $(\mathcal{C}^k, n)$-manifold $M$ which is covered by a family $\mathcal{F} = \{\mathcal{L}_\alpha\}_{\alpha \in A}$ of connected and disjointed $(\mathcal{C}^k, p)$-submanifolds such that, at any point $m$ in $M$, there exists a chart $(O_i, \Psi_i, U_i)$ and $\alpha$ in $A$ such that $m \in \mathcal{L}_\alpha \cap O_i$ and $\Psi_i(\mathcal{L}_\alpha \cap O_i) = U_i \cap F_\alpha$, where $F_\alpha$ is defined

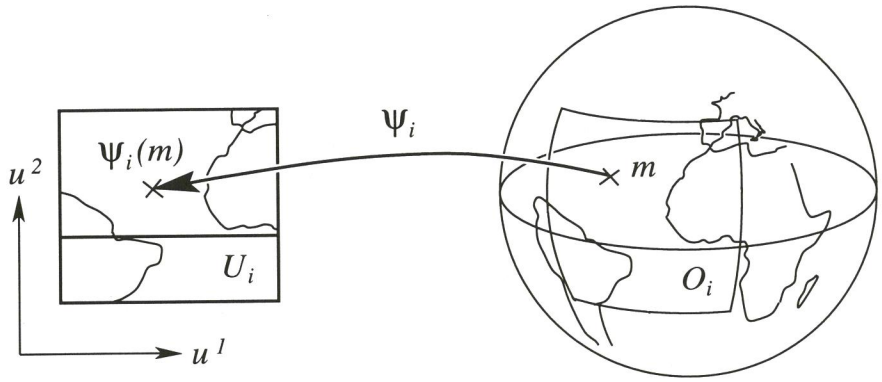


**Figure A1.** Manifold is a general concept that includes curves, surfaces and volumes as particular cases.

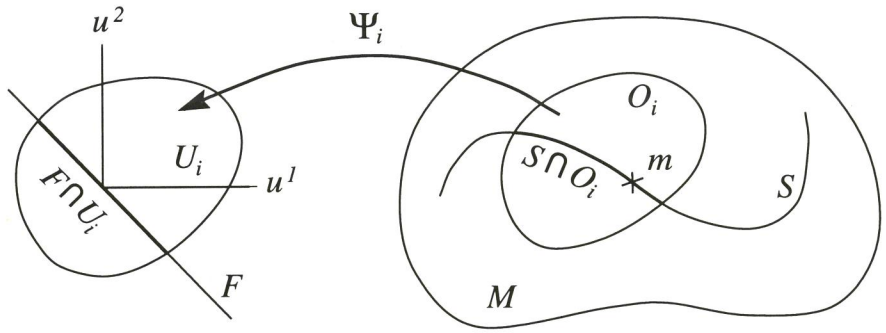


**Figure A2.** A submanifold is a subset of a manifold, which is also a manifold. Typically, curves and surfaces are submanifolds of the physical space.

by the $n-p$ equations $(u_i^{p+1} = \text{cst}\,(\alpha);\ \ldots;\ u_i^n = cst\,(\alpha))$, with $(u_i^1, \ldots, u_i^n)$ being a coordinate system in $U_i$. The $\mathscr{L}_\alpha$ are called the leaves of the *foliation* $\mathscr{F} = \{\mathscr{L}_\alpha\}_{\alpha \in A}$ (Fig. A3). Foliation $\mathscr{F}$ is said to be $p$-dimensional if $p$ is the dimension of its leaves.

In the context of geological modelling in sedimentary basins, we use these concepts as follows.

Euclidean *physical space* may be viewed as a $(\mathscr{C}^\infty, 3)$-manifold, simply by using the identity in $\mathscr{R}^3$ as a chart. The choice of an orthonormal frame results in a Cartesian coordinate system $(x^1, x^2, x^3)$ in physical space.

A piece $M$ of a *geological structure*, in which no fault or unconformity occurs, is considered as a $(\mathscr{C}^k, 3)$-submanifold in the physical space. We assume that $M$ can be described by only one chart $(M, \Psi, U)$, the inverse of which is viewed as a parametric representation $(U, \Phi = \Psi^{-1}, M)$. $\Phi$ maps any point whose curvilinear coordinates are $(u^1, u^2, u^3)$ in $U$ into a point with Cartesian coordinates $(x^1, x^2, x^3)$ in physical space, so that $M = \Phi(U)$. At each point $m$ in $M$ the tangent space $\mathbf{T}_m M$ is isometric to physical space $\mathscr{R}^3$.

Such a piece of a structure $M$ is foliated by a family $\mathscr{F} = \{\mathscr{L}_\alpha\}_{\alpha \in \mathscr{A}}$ of surfaces that represent *deposition isochrons*. According to the above definition of a foliation, we choose the curvilinear coordinate $u^3$ to index the leaves of $\mathscr{F}$. $\mathbf{T}_m \mathscr{F}_m$ is the tangent plane at $m$ to the leaf $\mathscr{F}_m$ of foliation $\mathscr{F}$ that contains point $m$. Via some monotonic function, $u^3$ may be interpreted as deposition time.

Finally, let us note that a foliated domain and its foliation leaves also inherit their metric properties from those of physical space via their respective tangent vector spaces.

We often use notations such as $\mathbf{T}M$ or $\mathbf{T}\mathscr{F}$ instead of $\mathbf{T}_m M$ or $\mathbf{T}_m \mathscr{F}_m$. The exact definition of the vector bundle $\mathbf{T}M$ can

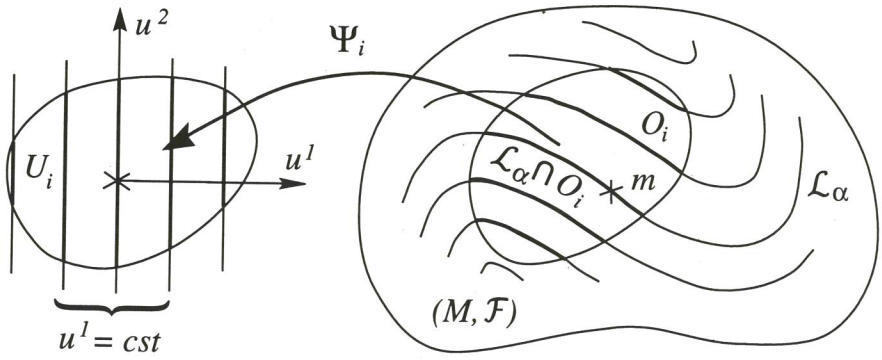


**Figure A3.** A foliation is a set of connected and disjointed submanifolds covering a manifold.

be found in Spivak (1979, Vol. I). Intuitively, it consists of the set of all the vectors that are somewhere tangent to $M$.

## APPENDIX B: CONVERGENCE VECTOR CONSERVATION DURING FOLDING

The paper-bound book analogy makes it clear that folding a parallel foliation yields another parallel foliation since length is conserved along the sheets and since their thickness is also conserved. Of course, the sheets should remain in contact.

We demonstrate two results here, which are based on rock volume conservation. The first result states that, if the foliation leaf area is conserved, then parallelism is conserved during folding. The second result states that, if length is conserved along the leaves of the foliation, then the deviation from parallelism, i.e. the convergence vector, is conserved.

### B.1 Notation

We consider two foliated domains $(M, \mathcal{F})$ and $(M', \mathcal{F}')$, which are embedded in the Euclidean physical space $\mathcal{R}^3$, and a $\mathcal{C}^2$-diffeomorphism $\varphi$ that maps $(M, \mathcal{F})$ on $(M', \mathcal{F}')$. $(M, \mathcal{F})$ (resp. $(M', \mathcal{F}')$) represents the initial (resp. final) state of a sedimentary block, and $\varphi$ represents folding (Fig. B1). Notations about tangent spaces are similar to those mentioned in Appendix A. We denote as $\langle , \rangle$ the usual scalar product in the Euclidean physical space. We choose a field of orthonormal bases $\{\mathbf{e}_1, \mathbf{e}_2\}$ (resp. $\{\mathbf{e}'_1, \mathbf{e}'_2\}$) in $\mathbf{T}\mathcal{F}$ (resp. $\mathbf{T}\mathcal{F}'$), and a field of orthonormal bases $\{\mathbf{e}_1, \mathbf{e}_2, \mathbf{e}_3\}$ (resp. $\{\mathbf{e}'_1, \mathbf{e}'_2, \mathbf{e}'_3\}$) in $\mathbf{T}M$ (resp. $\mathbf{T}M'$). We denote as $\mathbf{T}_\perp\mathcal{F}$ the field of vector subspaces in $\mathbf{T}M$, which are orthogonal to $\mathbf{T}\mathcal{F}$. Finally, we denote by $d\varphi$ the first derivative of $\varphi$, i.e. its Jacobian matrix if particular coordinates are chosen. $d\varphi$ maps linearly $\mathbf{T}M$ on $\mathbf{T}M'$ and $\mathbf{T}\mathcal{F}$ on $\mathbf{T}\mathcal{F}'$.

In this appendix, $\wedge$ denotes the wedge product (Spivak 1979, Vol. II) and should be distinguished from the usual cross product $\times$.

### B.2 Assumptions

The above physical assumptions are translated into mathematical terms as follows.

**(VC)** Volume conservation. $d\varphi(\mathbf{e}_1 \wedge \mathbf{e}_2 \wedge \mathbf{e}_3) = \mathbf{e}'_1 \wedge \mathbf{e}'_2 \wedge \mathbf{e}'_3$.

**(AC)** Area conservation in $\mathbf{T}\mathcal{F}$. $d\varphi(\mathbf{e}_1 \wedge \mathbf{e}_2) = \mathbf{e}'_1 \wedge \mathbf{e}'_2$.

**(LC)** Length conservation in $\mathbf{T}\mathcal{F}$. $d\varphi(\mathbf{e}_1) = \mathbf{e}'_1$ and $d\varphi(\mathbf{e}_2) = \mathbf{e}'_2$.

### B.3 Prerequisites

The following prerequisites will be used (see Spivak (1979, Vols I and II) for further details).

**(DD)** Directional derivative. See Section 4.1 in the main text.

**(BR)** Bracket. The bracket $[\mathbf{U}, \mathbf{V}]$ of two $\mathcal{C}^1$ vector fields $\mathbf{U}$ and $\mathbf{V}$ is a $\mathcal{C}^0$ vector field such that $[\mathbf{U}, \mathbf{V}] = D_\mathbf{U}\mathbf{V} - D_\mathbf{V}\mathbf{U}$.

**(FR)** Frobenius theorem. For any $\mathcal{C}^1$ vector fields $\mathbf{U}$ and $\mathbf{V}$ in $\mathbf{T}\mathcal{F}$, $(M, \mathcal{F})$ being a $(\mathcal{C}^k, n, p)$-foliation with $k \geq 2$, we have $[\mathbf{U}, \mathbf{V}] \in \mathbf{T}\mathcal{F}$.

**(PD)** Scalar product derivation formula. If $\mathbf{U}$ and $\mathbf{V}$ are $\mathcal{C}^1$ vector fields, then we have

$$(\mathbf{U}, \langle \mathbf{V}, \mathbf{W} \rangle) = \langle D_\mathbf{U}\mathbf{V}, \mathbf{W} \rangle + \langle \mathbf{V}, D_\mathbf{U}\mathbf{W} \rangle. \tag{B1}$$

**(DB)** Diffeomorphism and bracket. If $\varphi$ is a $\mathcal{C}^2$-diffeomorphism in $\mathcal{R}^3$ and if $\mathbf{U}$ and $\mathbf{V}$ are $\mathcal{C}^1$ vector fields, then $d\varphi([\mathbf{U}, \mathbf{V}]) = [d\varphi(\mathbf{U}), d\varphi(\mathbf{V})]$.

**(UN)** Unit vector field. If $\mathbf{U}$ is a unit $\mathcal{C}^1$ vector field and if $\mathbf{V}$ is a $\mathcal{C}^0$ vector field, then $D_\mathbf{V}\mathbf{U}$ is orthogonal to $\mathbf{U}$ for any $\mathbf{V}$. Indeed, we have $(\mathbf{V} \cdot \langle \mathbf{V}, \mathbf{U} \rangle) = (\mathbf{V} \cdot 1) = 0$, and from the **(PD)** formula we obtain $(\mathbf{V} \cdot \langle \mathbf{U}, \mathbf{U} \rangle) = 2\langle D_\mathbf{V}\mathbf{U}, \mathbf{U} \rangle$, so that $\langle D_\mathbf{V}\mathbf{U} \cdot \mathbf{U}, \mathbf{U} \rangle = 0$.

**(DV)** Diffeomorphism and vector product. If $\mathbf{\Omega}$ and $\mathbf{\Theta}$ are two continuous covector fields and if $\varphi$ is a $\mathcal{C}^1$-diffeomorphism, then $d\varphi(\mathbf{\Omega} \wedge \mathbf{\Theta}) = d\varphi(\mathbf{\Omega}) \wedge d\varphi(\mathbf{\Theta})$.

### B.3 Theorem (B1)

*Under assumptions* **(VC)** *and* **(AC)**, *we have*

$$\langle d\varphi(\mathbf{Y}), D_{\mathbf{e}'_3}\mathbf{e}'_3 \rangle = \langle \mathbf{Y}, D_{\mathbf{e}_3}\mathbf{e}_3 \rangle \tag{B2}$$

*for any* $\mathcal{C}^1$ *vector field* $\mathbf{Y}$ *in* $\mathbf{T}\mathcal{F}$.

Since $D_{\mathbf{e}_3}\mathbf{e}_3$ is the convergence vector before folding, this means that initial parallelism ($D_{\mathbf{e}_3}\mathbf{e}_3 = 0$) is conserved after folding ($D_{\mathbf{e}'_3}\mathbf{e}'_3 = 0$).

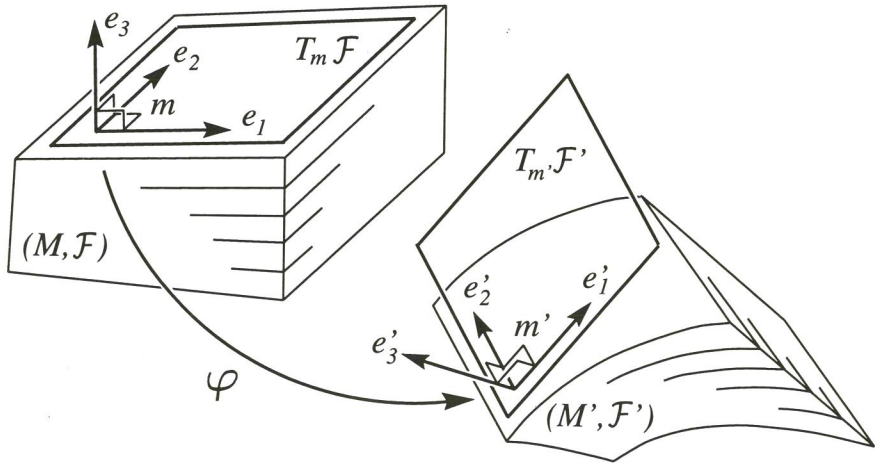


**Figure B1.** Folding of sedimentary rocks can be viewed as a diffeomorphism between foliations.

### B.4 Proof of theorem (B1)

$$\mathbf{e}'_1 \wedge \mathbf{e}'_2 \wedge \mathbf{e}'_3 \overset{(\mathbf{VC})}{=} d\varphi(\mathbf{e}_1 \wedge \mathbf{e}_2 \wedge \mathbf{e}_3)$$

$$\overset{(\mathbf{DV})}{=} d\varphi(\mathbf{e}_1 \wedge \mathbf{e}_2) \wedge d\varphi(\mathbf{e}_3)$$

$$\overset{(\mathbf{AC})}{=} \mathbf{e}'_1 \wedge \mathbf{e}'_2 \wedge d\varphi(\mathbf{e}_3) \tag{B3}$$

Hence, there exists a vector field $\mathbf{X}'$ in $\mathbf{T}\mathscr{F}'$ such that

$$d\varphi(\mathbf{e}_3) = \mathbf{e}'_3 + \mathbf{X}'. \tag{B4}$$

Let us now evaluate the equation $E = \langle d\varphi(\mathbf{Y}), d\varphi(\mathbf{e}_3)], \mathbf{e}'_3\rangle$ in which the vector field $\mathbf{Y}$ is in $\mathbf{T}\mathscr{F}$.

$$E \overset{(\mathbf{B4})}{=} \langle [d\varphi(\mathbf{Y}), \mathbf{e}'_3], \mathbf{e}'_3 > + \langle [d\varphi(\mathbf{Y}), \mathbf{X}'], \mathbf{e}'_3\rangle$$

$$\overset{(\mathbf{FB})}{=} \langle [d\varphi(\mathbf{Y}), \mathbf{e}'_3], \mathbf{e}'_3\rangle$$

$$\overset{(\mathbf{BR})}{=} \langle D_{d\varphi(\mathbf{Y})}\mathbf{e}'_3, \mathbf{e}'_3\rangle - \langle D_{\mathbf{e}'_3} d\varphi(\mathbf{Y}), \mathbf{e}'_3\rangle$$

$$\overset{(\mathbf{UN})}{=} - \langle D_{\mathbf{e}'_3} d\varphi(\mathbf{Y}), \mathbf{e}'_3\rangle$$

$$\overset{(\mathbf{PD})}{=} - \mathbf{e}'_3 \cdot \langle d\varphi(\mathbf{Y}), \mathbf{e}'_3\rangle + \langle d\varphi(\mathbf{Y}), D_{\mathbf{e}'_3}\mathbf{e}'_3\rangle$$

$$= \langle d\varphi(\mathbf{Y}), D_{\mathbf{e}'_3}\mathbf{e}'_3\rangle. \tag{B5}$$

By, splitting $[\mathbf{Y}, \mathbf{e}_3]$ into two vector fields, parallel and orthogonal to $\mathbf{T}\mathscr{F}$, we obtain

$$E = \langle d\varphi([\mathbf{Y}, \mathbf{e}_3]_{\mathbf{T}^\perp\mathscr{F}}), \mathbf{e}'_3\rangle + \langle d\varphi([\mathbf{Y}, \mathbf{e}_3]_{\mathbf{T}\mathscr{F}}), \mathbf{e}'_3\rangle$$
$$= \langle d\varphi(\langle [\mathbf{Y}, \mathbf{e}_3], \mathbf{e}_3\rangle \mathbf{e}_3), \mathbf{e}'_3\rangle$$
$$= \langle [\mathbf{Y}, \mathbf{e}_3], \mathbf{e}_3\rangle \langle d\varphi(\mathbf{e}_1), \mathbf{e}'_3\rangle$$

$$\overset{(\mathbf{B4})}{=} \langle [\mathbf{Y}, \mathbf{e}_3], \mathbf{e}_3\rangle \langle \mathbf{e}'_3 + \mathbf{X}', \mathbf{e}'_3\rangle$$

$$= \langle \mathbf{Y}, \mathbf{e}_3], \mathbf{e}_3\rangle$$

$$\overset{(\mathbf{BR})}{=} \langle D_{\mathbf{Y}}\mathbf{e}_3, \mathbf{e}_3\rangle - \langle D_{\mathbf{e}_3}\mathbf{Y}, \mathbf{e}_3\rangle$$

$$\overset{(\mathbf{UN})}{=} - \langle D_{\mathbf{e}_3}\mathbf{Y}, \mathbf{e}_3\rangle$$

$$\overset{(\mathbf{PD})}{=} \mathbf{e}_3\langle \mathbf{Y}, \mathbf{e}_3\rangle + \langle \mathbf{Y}, D_{\mathbf{e}_3}\mathbf{e}_3\rangle$$

$$= \langle \mathbf{Y}, \mathbf{D}_{\mathbf{e}_3}\mathbf{e}_3\rangle. \tag{B6}$$

Connecting eqs (B5) and (B6) concludes the proof.

### B.5 Theorem (B2)

*Under assumptions* **(VC)** *and* **(LC)**, *we have*

$$\begin{cases} \langle \mathbf{e}'_1, D_{\mathbf{e}'_3}\mathbf{e}'_3\rangle = \langle \mathbf{e}_1, D_{\mathbf{e}_3}\mathbf{e}_3\rangle \\ \langle \mathbf{e}'_2, D_{\mathbf{e}'_3}\mathbf{e}'_3\rangle = \langle \mathbf{e}_2, D_{\mathbf{e}_3}\mathbf{e}_3\rangle. \end{cases} \tag{B7}$$

This means that the components of convergence vector $D_{\mathbf{e}_3}\mathbf{e}_3$ are the same in the base $\{\mathbf{e}_i\}$ before folding as those of $D_{\mathbf{e}'_3}\mathbf{e}'_3$ in the base $\{\mathbf{e}'_i\}$ after folding. In that sense, the convergence vector is conserved because $\{\mathbf{e}_1, \mathbf{e}_2\}$ and $\{\mathbf{e}'_1, \mathbf{e}'_2\}$ are both orthonormal and hence isometric.

### B.6 Proof of theorem (B2)

Since **(LC)** implies **(AC)**, Theorem (B1) holds. By virtue of **(LC)**, choosing $\mathbf{e}_1$ and $\mathbf{e}_2$ as particular instances of $\mathbf{Y}$ in eq. (B2) concludes the proof.

## APPENDIX C: MATHEMATICAL BASIS OF THE ADDITIONAL CRITERION METHOD

Here we state two lemmas and a theorem, which assess the additional criterion method. The first lemma states that optimizing parametric representations instead of foliations still enables the optimal foliation(s) to be found. The second lemma states that the additional criterion method, including the projection step, keeps the original physical problem unchanged. The theorem states that a (strictly) unphysical objective function does exist after the projection step.

### C.1 Notation

We denote by $M_\Phi$ the set of the admissible parametric representations and by $M_\mathscr{F}$ the set of the admissible foliations. We consider the map

$$s : \Phi \in M_\varphi \to \mathscr{F} = s(\Phi) \in M_\mathscr{F}, \tag{C1}$$

which maps a parametric representation $\Phi$ on the foliation $\mathscr{F}$ represented by $\Phi$.

### C.2 Assumptions

**(PR)** Parametric representations. We recall that a foliated domain $(M, \mathscr{F})$ in $\mathscr{R}^3$ is described by a parametric representation $\Phi$, i.e. a $\mathscr{C}^2$-diffeomorphism between $U = [0, 1]^3$ and $M \subset \mathscr{R}^3$:

$$\varphi : \mathbf{u} = (u^1, u^2, u^3) \in U \to \Phi(\mathbf{u}) = (x^1, x^2, x^3). \tag{C2}$$

**(MP)** Manifold of parametric representations. $M_\Phi$ is a Banach manifold, i.e. an infinite dimensional manifold. Note that $M_\Phi$ is not a vector space since parametric representations are diffeomorphisms and since zero is not a diffeomorphism.

**(MF)** Manifold of foliations. $M_\mathscr{F}$ is also a manifold which can be viewed as the quotient space $M_\Phi/\sim$ of $M_\Phi$ by the equivalence relation $\sim$ defined by

$$\{\Phi_1 \sim \Phi_2\} \Leftrightarrow \{s(\Phi_1) = s(\Phi_2)\}. \tag{C3}$$

**(FI)** Fibration of equivalence classes. The equivalence relation $\sim$ builds a foliation $\mathscr{M}$ on $M_\Phi$.

**(DI)** Differentiability. Manifolds $M_\Phi$ and $M_\mathscr{F}$ as well as map $s$ and foliation $\mathscr{M}$ are differentiable.

**(SU)** Submersion. The map $s$ is a submersion, i.e. $s$ is surjective as well as $ds$:

$$(ds)_\Phi : \mathbf{X} \in \mathbf{T}_\Phi M_\Phi \to \mathbf{Y} = (ds)_\Phi \mathbf{X} \in \mathbf{T}_{s(\Phi)} M_\mathscr{F}, \tag{C4}$$

where $\mathbf{X}$ and $\mathbf{Y}$ may be interpreted as perturbations of $\Phi$ and $\mathscr{F}$ respectively. As a result, $\mathbf{T}\mathscr{M} = \ker(ds)$.

### C.3 Lemma (C1)

*If $s$ is a submersion from $M_\Phi$ to $M_\mathcal{F}$, if $Q_\varphi$ is a function defined on $M_\mathcal{F}$, and if $\Phi$ is a critical point of $Q_\varphi \circ s$,* i.e. *$d(Q_\varphi \circ s)_\Phi = 0$, then $s(\Phi)$ is a critical point of $Q_\varphi$.*

$Q_\varphi$ is the physical objective function defined for foliations, and $Q_\varphi \circ s$ is the physical objective function defined for parametric representations.

### C.4 Proof of lemma (C1)

We have $d(Q_\varphi \circ s)_\Phi = d(Q_\varphi)_{s(\Phi)} \circ (ds)_\Phi$. $\Phi$ is a critical point of $Q_\varphi \circ s$ if and only if $d(Q_\varphi \circ s)_\Phi = 0$, i.e. $(dQ_\varphi)_{s(\Phi)} \circ (ds)_\Phi = 0$. Since $(ds)_\Phi$ is surjective, this is equivalent to $(dQ_\varphi)_{s(\Phi)} = 0$, i.e. $s(\Phi)$ is a critical point of $Q_\varphi$.

### C.5 Lemma (C2)

*We consider the situation of lemma* 1 *and a function $Q_\alpha$ defined on $M_\Phi$*

$$\begin{array}{ccc} M_\Phi & \xrightarrow{Q_\alpha} & \mathcal{R} \\ \downarrow s & & \\ M_\mathcal{F} & \xrightarrow{Q_\varphi} & \mathcal{R}. \end{array} \tag{C5}$$

*We consider $\mathbf{T}^s\mathcal{M}$, a supplementary of $\mathbf{T}\mathcal{M}$ in $\mathbf{T}M_\Phi$, and we define the differential* 1*-form $\omega$ on $\mathbf{T}M_\Phi$ as follows*

$$\begin{cases} \omega = \mathrm{d}Q_\alpha & \text{on } \mathbf{T}\mathcal{M} \\ \omega = 0 & \text{on } \mathbf{T}^s\mathcal{M}. \end{cases} \tag{C6}$$

*If $\Phi$ in $M_\Phi$ such that $\omega_\Phi + \mathrm{d}(Q_\varphi \circ s)_\Phi = 0$, then $s(\Phi)$ is a critical point of $Q_\varphi$.*

This means that the additional criterion method, including the projection step, does not disturb the physical problem.

### C.6 Proof of lemma (C2)

Since $\mathbf{T}^s\mathcal{M} \oplus \mathbf{T}\mathcal{M} = \mathbf{T}\mathcal{M}_\Phi$ and $ds = 0$ on $\mathbf{T}\mathcal{M}$, for any $\mathbf{Y}$ in $\mathbf{T}_{s(\Phi)}M_\mathcal{F}$, there exists $\mathbf{X}$ in $\mathbf{T}^s\mathcal{M}$ such that $ds_\Phi \cdot \mathbf{X} = \mathbf{Y}$. Since $\omega_\Phi + d(Q_\alpha \circ s)_\Phi = 0$, and since $\omega_\Phi \cdot \mathbf{X} = 0$ because $\mathbf{X} \in \mathbf{T}^s\mathcal{M}$, we have $d(Q_\varphi \circ s)_\Phi \cdot \mathbf{X} = 0$. Using lemma 1 concludes the proof, that is $s(\Phi)$ is a critical point of $Q_\varphi$.

### C.7 Theorem (C1)

*Let $(M_\Phi, \mathcal{M})$ be a manifold endowed with a foliation $\mathcal{M}$. We assume that $M_\Phi$ is endowed with a* 1*-form $\omega$ whose restriction $\omega_{|\mathrm{F}}$ to each leaf* F *of $\mathcal{M}$ is closed (this is the situation of lemma* C2, *eq.* C6*). Then, locally, $M_\Phi$ admits a closed form $\tilde{\omega}$ whose restriction $\tilde{\omega}_{|\mathrm{F}}$ to each leaf* F *of $\mathcal{M}$ equals $\omega_{|\mathrm{F}}$.*

The 1-form $\tilde{\omega}$ is the gradient of what is called $Q_\alpha^\mathrm{p}$ in the main text. Since $\tilde{\omega}$ is closed, then $Q_\alpha^\mathrm{p}$ does exist locally.

### C.8 Proof of theorem (C1)

Let $m \in M_\Phi$, and $V$ be a neighbourhood of $m$. Let $G$ be a smooth submanifold, transversal to $\mathcal{M}$ ($G$ cuts each leaf once).

We define a function $f_F$ on the leaf $F$ in the following way. Let $u \in F$ and $a \in G \cap F$. Let $\gamma$ be a curve on $F$ with endpoints $a$ and $u$. We set (along $\gamma$)

$$f_F(u) = \int_a^u \omega_{|F}(x)\, dx. \tag{C7}$$

Since $\omega_{|F}$ is closed on $F$, the integral is independent of $\gamma$. Now, we define $f$ on $V$ by $f(x) = f_F(x)$ if $x \in F$. Since $G$ and $\omega$ are smooth, then $f$ is smooth. Let $\tilde{\omega} = df$. We need to check that the restriction $\tilde{\omega}_{|F}$ of $\tilde{\omega}$ to each leaf $F$ equals $\omega_{|F}$. We have, for any vector field $\mathbf{X}$ in $\mathbf{T}\mathcal{M}$, $\tilde{\omega}_{|F}(\mathbf{X}) = d_\mathcal{M} f(\mathbf{X})$, since $\mathbf{X}$ is tangent to $\mathcal{M}$. Therefore, $\tilde{\omega}_{|F}(\mathbf{X}) = (\mathbf{X} \cdot f) = \omega_{|F}(\mathbf{X})$ and finally $\tilde{\omega}_{|F} = \omega_{|F}$.

## APPENDIX D: NECESSITY OF THE PROJECTION STEP

Here we describe two numerical experiments that demonstrate the necessity of the projection step in the additional criterion method.

Figure D1 (opposite p. 75) shows the initial model of the inversion. This inversion consists of optimizing layer parallelism over all the foliation, with its top surface being given, as well as the intersections of its leaves with the vertical well. Of course, the final model is expected to remain the same.

Nevertheless, if we 'forget' to project Jacobian matrix $\mathbf{J}_\alpha$, the resulting foliation is not parallel, as is visible in Fig. D2 (opposite p. 75). We explain this fact as follows. Since the constraint points are such that the quantity $\dfrac{\partial \Phi^3}{\partial u^3}$ is not a constant in the well, $\dfrac{\partial^2 \Phi^3}{\partial u^3\, \partial u^3}$ is not zero at these locations. Far from the well, however, the additional criterion makes the mesh more regular and $\dfrac{\partial^2 \Phi^3}{\partial u^3\, \partial u^3}$ close to zero, and consequently the foliation is not parallel.

Using the projected Jacobian matrix $\mathbf{J}_\alpha^\mathrm{p}$ and the model shown in Fig. D2 as the initial model, the inversion again yields the expected model shown in Fig. D1.